Astron. Astrophys. 313, 545–564 (1996)

ASTRONOMY AND ASTROPHYSICS

The TP-AGB phase: a new model

P. Marigo[1], **A. Bressan**[2], **and C. Chiosi**[1]

[1] Department of Astronomy, University of Padova, Vicolo dell'Osservatorio 5, I-35122 Padova, Italy
[2] Astronomical Observatory, Vicolo dell'Osservatorio 5, I-35122 Padova, Italy

Received 28 August 1995 / Accepted 28 February 1996

Abstract. This study deals with the TP-AGB phase of low and intermediate-mass stars ($0.7 \lesssim M/M_{\odot} \lesssim 5$). To this aim, a semi-analytical model is constructed. A representative set of TP-AGB evolutionary models is calculated for two classes of initial metallicity ($Z = 0.02$ and $Z = 0.008$). A detailed analysis is performed to estimate the changes in the surface chemical composition caused by (1) the inter-shell nucleosynthesis and convective dredge-up; (2) nuclear burning in the deepest layers of the convective envelope; and (3) mass loss by stellar wind. The evolution of the abundances of 13 chemical elements (H, ^{3}He, ^{4}He, ^{12}C, ^{13}C, ^{14}N, ^{15}N, ^{16}O, ^{17}O,^{18}O, ^{20}Ne, ^{22}Ne, ^{25}Mg) is followed.

In particular, the formation of carbon stars is investigated. We use the observed luminosity function of carbon stars in the LMC as the constraint whose fulfillment determines the values of the parameters adopted in the model, namely: the minimum core mass for dredge-up $M_{\rm c}^{\rm min}$ and the efficiency of the third dredge-up λ. In this way, we derive a proper calibration which the reliability of the chemical analysis stands on.

We calculate the stellar yields for both metallicities to provide new data for these key-ingredients in the process of chemical enrichment of the interstellar medium. The chemical composition of PNe is derived and compared to the latest experimental data both in the Galaxy and in the LMC, which leads to a partial agreement. Observed information on the correlation between luminosity and pulsational period of Mira and OH/IR variables is used to test further our results. Finally, we predict the initial-final mass relation and we compare it to the semi-empirically determined one for the solar neighbourhood. The agreement turns out to be satisfactory.

Key words: stars: evolution – stars: asymptotic giant branch – nuclear reactions, nucleosynthesis – stars: abundances – ISM: planetary nebulae: general

Send offprint requests to: P. Marigo

1. Introduction

In this paper we present a semi-analytical model to calculate the last evolutionary stages of low and intermediate- mass stars ($0.7 \lesssim M/M_{\odot} \lesssim 5$).

According to the usual classification (Chiosi et al. 1992) these stars, following core He-exhaustion, develop a degenerate carbon-oxygen core and during the ascent of the asymptotic giant branch (AGB) they experience helium shell flashes (Thermally Pulsing AGB or TP-AGB phase).

Our model primarily deals with the TP-AGB evolution. Given the initial conditions at the first thermal pulse, the calculation is carried on until one of the two alternatives is met: i) complete ejection of the envelope by stellar wind; or ii) growth of the core mass up to the Chandrasekhar limit ($\sim 1.4\ M_{\odot}$).

Our present understanding of the AGB phase has its roots in the pioneer works of Iben (1977) and Iben & Truran (1978), followed by the semi-analytical analysis of Renzini & Voli (1981; hereafter RV). Here, a particular care is devoted to the nucleosynthetic aspect so as to provide stellar yields, currently used in evolutionary models of galaxies.

The formal structure of the present model closely resembles the one of RV, our major contribution being an updating of the physical treatment, for we can benefit from the improvement achieved over these years by several theoretical investigations of the TP-AGB phase (Boothroyd & Sackmann 1988a-d, hereafter BSa-d; Vassiliadis & Wood 1993, hereafter VW; Groenewegen & de Jong 1993, hereafter GdJ; Groenewegen & de Jong 1994ab; see also the other studies referenced in the following).

The major implementations regard: the core mass-luminosity and the core mass-interpulse period relations in which a composition dependence is included; the mass loss formalism that establishes a realistic link between the mass-loss rate and the pulsation period of variable AGB stars; the inclusion of flash-driven luminosity variations; the adoption of revised nuclear reaction rates.

We particularly direct our effort to a quantitative determination of the variations in the surface chemical composition due to two different mechanisms, namely: i) the third dredge-up which corresponds to the inward penetration of the convective envelope and the mixing to the surface of nuclearly processed

material; and ii) envelope burning via the CNO cycle in the deepest layers of the convective envelope if a sufficiently high temperature is reached ($\geq 40 \times 10^6$ K).

The effect of the third dredge-up is analytically evaluated. The free parameters are the minimum core mass for dredge-up $M_c^{\rm min}$, and the third dredge-up efficiency λ. The chemical composition of the dredged-up material consists mainly of helium, carbon and oxygen. In particular, carbon enrichment can lead to the formation of carbon stars.

Envelope burning is included in a detailed way. A convective envelope model is used to obtain the stratification in temperature and density so that local CNO reaction rates are evaluated. When significant nuclear burning occurs, the surface abundances of ^{13}C and ^{14}N are enhanced at the expenses of ^{12}C and ^{16}O.

In this paper we follow the TP-AGB evolution of a representative set of stellar masses ($0.7 \lesssim M/M_\odot \leq 4$) for two different initial compositions with metallicity $Z = 0.02$ and $Z = 0.008$ (in mass fraction). The above upper limit of the mass range reflects the effect of the convective overshoot included in the complete evolutionary calculations employed as the starting point of our TP-AGB semi-analytical model. The reader can refer to Sect. 2.1 for a more exhaustive explanation of this point.

The principal applications and results of the present study can be summarized as follows:

- Calibration of the third dredge-up parameters ($M_c^{\rm min}$ and λ) on the base of the observed luminosity function of carbon stars in the LMC. A satisfactory fit is obtained assuming $M_c^{\rm min} = 0.58\ M_\odot$ and $\lambda = 0.65$. The value of the efficiency λ turns out to be much higher than the estimate resulting from complete evolutionary calculations ($\lambda \sim 0.3$).
- Evolutionary tracks in the HR diagram.
- Prediction of the initial-final mass relation.
- Analysis of the variations in the surface abundances of 13 chemical elements (H, ^{3}He, ^{4}He, ^{12}C, ^{13}C, ^{14}N, ^{15}N, ^{16}O, ^{17}O,^{18}O, ^{20}Ne, ^{22}Ne, ^{25}Mg).
- Stellar yields in which the contributions to the ejection of newly processed material during the RGB phase and AGB phase are included.
- Planetary nebulae (PNe) chemical composition.

In Sect. 2 the model is described; the results are presented and discussed in Sect. 3; final remarks are suggested in Sect. 4.

2. The TP-AGB model

To follow the evolution along the TP-AGB phase a semi-analytical method is adopted (RV; GdJ). The basic assumptions and physical prescriptions which the model stands on are described in the following subsections. They are:

1. initial conditions at the first thermal pulse;
2. analytical laws, derived from complete evolutionary calculations; to express:
   - the core mass-luminosity relation ($M_c - L$);
   - the core mass-interpulse period relation ($M_c - T_{\rm ip}$);
   - the rate of evolution along the TP-AGB;
   - the third dredge-up;
3. a semi-empirical prescription to evaluate the mass-loss rate by stellar wind;
4. a numerical algorithm to calculate:
   - the effective temperature;
   - CNO-burning possibly occurring at the base of convective envelope (envelope burning).

2.1. The initial conditions

The quantities that govern the physical condition of a star at the beginning of its TP-AGB phase are the total mass M, the core mass M_c, the luminosity L, the effective temperature $T_{\rm eff}$ and the chemical composition of the envelope.

We extract the initial conditions of a representative set of stellar masses ($0.7 \lesssim M/M_\odot \leq 4$) from the complete evolutionary tracks of Bressan et al. (1993) for $Z = 0.02$ and of Fagotto et al. (1994) for $Z = 0.008$. The tracks span a wide range of initial masses, from 0.6 $M_\odot$ to 120 $M_\odot$, and extend from the zero age main sequence (ZAMS) till very advanced evolutionary phases.

Specifically, low and intermediate-mass stars are followed till the beginning of the TP-AGB phase with the inclusion of the first few pulses. The models are calculated at constant mass, so that mass loss by stellar wind during the RGB and AGB phases may be included in an analytical fashion following the method outlined long ago by Renzini (1977). In particular, mass loss on the RGB can be easily accounted for by scaling the total mass of the star at the RGB tip down to the value suited to the horizontal branch (HB) stars (see Iben 1991). Actually, in the case of low-mass stars – those which experience the helium-flash at the RGB tip – the evolutionary tracks are not followed through the helium-flash, but zero age horizontal branch (ZAHB) models with the same He-core mass as at the tip of the RGB, no electron degeneracy, and different masses of the H-rich envelope are calculated and followed through the phase of core He-burning up to the start of the TP-AGB phase.

It is worth recalling that these models predict the changes in the surface abundance of 13 different chemical elements (H, ^{3}He, ^{4}He, ^{12}C, ^{13}C, ^{14}N, ^{15}N, ^{16}O, ^{17}O,^{18}O, ^{20}Ne, ^{22}Ne, ^{25}Mg) induced by the first and the second dredge-up episodes. For more details on the physical ingredients of the models see the complete description in the papers referenced above.

To find the starting conditions of the TP-AGB phase, we adopt the following criterium. For each mass we single out the first significant helium-shell flash, usually defined as the first pulse in which the flash strength $L_{\rm He}^{\rm max}$ exceeds the surface luminosity L (BSc). Hence, all the variables of interest are evaluated at the point just preceding the flash, that is the pre-flash luminosity maximum in the light curve (BSa).

It is important to stress that the initial conditions at the first thermal pulse globally reflect the past evolutionary history since the star settled on the ZAMS and, in this view, they play a fundamental role on the subsequent stages of the star evolution.

As far as our study is concerned, a notable point to recall is the inclusion of the convective overshoot (Chiosi et al. 1992)

in the complete evolutionary calculations we use as the starting point of the TP-AGB models. A crucial effect is that of lowering the critical value of the initial mass M_{up} over which carbon ignition occurs in non degenerate condition. Thus, M_{up} determines the maximum initial mass of a star which can pass through the double-shell phase.

The classical models without overshoot predict $M_{up} = 7 - 9\ M_{\odot}$, while the models with convective overshoot have a lower critical mass, $M_{up} = 5 - 6\ M_{\odot}$. That is the reason why our TP-AGB models present a narrower range of initial stellar masses ($\leq 5 M_{\odot}$) if compared to those of RV ($\leq 8 M_{\odot}$) where no overshoot is taken into account. This circumstance could have a strong impact on the predicted high luminosity tail of the luminosity function of carbon stars in the LMC (see Sect. 3.6).

2.2. The core mass-luminosity relation

The $M_c - L$ relation relates the quiescent luminosity L of an AGB star to its core mass M_c during the interpulse period, where M_c is traditionally defined as the mass M_H interior to the hydrogen-burning shell. Paczynski (1970) first derived a linear law from his evolutionary calculations and since then various theoretical investigations have confirmed the existence of a $M_c - L$ relation for the AGB phase (Iben 1977; Havazelet & Barkat 1979; Wood & Zarro 1981; Lattanzio 1986; BSb).

On the other hand, recent studies show that the validity of such a relation is conditioned to the efficiency of envelope burning, which may produce a significant overluminosity in AGB stars of higher mass (Blöcker & Schönberner 1991; Lattanzio 1992; Boothroyd & Sackmann 1992; Blöcker 1995; see also Sect. 3.1.2).

In this work we use the following two $M_c - L$ relations which include the dependence on the chemical composition:

$$L = 238\,000 \mu^3 Z_{CNO}^{0.04} (M_c^2 - 0.0305 M_c - 0.1802) \quad (1)$$

for stars with a core mass in the range $0.5 \leq M_c/M_{\odot} \leq 0.66$ (presented in BSb); and

$$L = 122585 \mu^2 (M_c - 0.46) M^{0.19} \quad (2)$$

for stars with core mass $M_c/M_{\odot} \geq 0.95$ (originally from Iben & Truran (1978) according to the slightly modified version of GdJ, see also Iben (1977)).

In these formulas stellar masses M and luminosities L are in solar units; Z_{CNO} is the total abundance (in mass fraction) of carbon, nitrogen and oxygen in the envelope; $\mu = 4/(5X+3-Z)$ is the mean molecular weight for a fully ionized gas, where X and Z are the hydrogen and metal abundances, respectively. For stars with $0.66 \leq M_c/M_{\odot} \leq 0.95$ a linear interpolation is adopted.

Care is taken to evaluate the overluminosity L_{CNO} due to envelope burning and to check its relative contribution to the stellar luminosity L. We anticipate that during calculations L_{CNO}/L is never found to exceed few percents, except for the ($4\ M_{\odot}$, $Z = 0.008$) model (see Sect. 3.1.2).

2.3. The core mass-interpulse period relation

The time-scale characteristic of a thermal pulse, T_{ip}, that is the time interval (interpulse period) between two subsequent pulses, is a decreasing function of the core mass (Paczynski 1975).

We use the results of the theoretical investigation of BSc. Quite a strong dependence on composition emerges: at the same core mass, T_{ip} for the low metallicity case (e.g. $Z = 0.001$) is found to be nearly twice longer than in the high metallicity case (e.g. $Z = 0.02$):

$$\log T_{ip} = \begin{cases} 4.50(1.689 - M_c) & Z = 0.02 \\ 4.95(1.644 - M_c) & Z = 0.001 \end{cases} \quad (3)$$

For other metallicities, we linearly interpolate between the above relations using $\log Z$ as the independent variable.

2.4. The rate of evolution

The inter-flash luminosity is mostly generated by the hydrogen-burning shell, via the CNO cycle, so that the evolution of a star along the TP-AGB phase is governed by the rate of core mass growth.

For our model we use the analytical law suggested by GdJ:

$$\frac{dM_c}{dt} = 9.555\ 10^{-12}\ \frac{L_H}{X} \quad (4)$$

where M_c is the core mass (in solar masses), X is the hydrogen abundance (in mass fraction) in the envelope, L_H is the luminosity produced by H-burning (in solar units). The numerical factor gives the energy released from the nuclear conversion of 1 g of hydrogen ($\sim 6.4\ 10^{18}$ erg).

To include the small contribution (few percents) from He-burning and gravitational contraction of the core to the total luminosity we adopt the following relation (Iben 1977; see also GdJ):

$$L = L_H + 2000\ (M/7)^{0.4}\ \exp[3.45\ (M_c - 0.96)] \quad (5)$$

All the variables are expressed in solar units.

2.5. The first pulses

Both the $M_c - L$ relation and the $M_c - T_{ip}$ relation correctly describe the behavior of thermal pulses after they reach full amplitude (Iben & Renzini 1983).

Before that, the characteristic trend of the first pulses is significantly different. Firstly, the onset of the helium-shell flashes occurs at a lower luminosity than that one expected by the $M_c - L$ relation. We do verify this feature belongs to every evolutionary track we extract the initial conditions from.

Secondly, the growth of luminosity is steeper for the first pulses until the flash strength – the peak flash helium-burning luminosity L_{He}^{max} – approaches its asymptotic value, at which point pulses are generally considered to have reached "full amplitude". Actually, this does not correspond to a constant value of L_{He}^{max}, but it means only that the flash strength grows slower

than exponentially, so that also the increase of stellar luminosity flattens out.

To mimic this trend we use the results of the evolutionary calculations of VW and derive a simple linear law which gives the suitable increase in luminosity as a function of the core mass increment, the slope depending on the mass of the star.

Concerning the interpulse period $T_{\rm ip}$ of the first pulses, it is found to be much shorter if compared to the corresponding value given by Eqs. (3). We take into account this effect by adopting the corrections tabulated in Table 1 of GdJ.

2.6. Flash-driven luminosity variations

The existence of flash-driven luminosity variations is well established by theoretical investigations of thermal pulses. The occurrence of such events makes the star depart from the standard $M_{\rm c} - L$ relation (BSa).

The main deviations in the light curve occur at the peak flash luminosity directly following a thermal pulse and during the subsequent long-lived luminosity-dip. The former corresponds to a sudden and brief ($\sim 1\%$ of $T_{\rm ip}$) increase of the luminosity over its quiescent value as an effect of the inner thermal runaway on the surface layers, which are forced to expand. The latter reflects the declining of the helium-burning luminosity that causes low mass stars to spend as much as $20 - 30\%$ of the interpulse period at a luminosity a factor 2 lower than the value predicted by the $M_{\rm c} - L$ relation. In this study we take into account such significant luminosity variations following the analytical prescriptions in GdJ.

2.7. Mass loss

Mass loss by stellar wind plays a crucial role on the evolution of an AGB star, since it not only determines the final mass at the tip of the AGB and hence the maximum luminosity, but it also affects the internal structure and nucleosynthesis.

To this respect, a systematic study has been developed by Groenewegen & de Jong (1994b). They analyse the sensitivity of their results on different mass loss laws, which they alternate in the analytical AGB evolutionary calculations. More recently, Blöcker (1995) has suggested a formula to evaluate the mass-loss rate, based on dynamical calculations of the atmosphere of Mira-like stars by Bowen (1988). The investigation is directed to point out the influence of the mass loss on different aspects of the AGB evolution. A notable point is the close connection between envelope burning and mass loss. The strength of the wind can weaken the overluminosity produced by envelope burning (see Sect. 3.1.2).

In our TP-AGB model we adopt a semi-empirical formalism which relates the mass loss rate $\dot{M}$ to the pulsation period P (VW). It has been derived from observational determinations of mass-loss rates for Mira variables and pulsating OH/IR stars both in the Galaxy and in the LMC.

The notable feature of this prescription is the onset of the superwind which develops naturally on the AGB, instead of the artificial sudden transition that is needed if a Reimers-like law for $\dot{M}$ is used (RV).

Two distinct phases of mass loss are considered. For periods shorter than 500 days $\dot{M}$ increases exponentially with P (Mira phase), while beyond this limit the mass-loss rate is practically constant at values typical of the superwind (few times 10^{-5} $M_\odot\,{\rm yr}^{-1}$). The adopted relations are:

$$\log \dot{M} = -11.4 + 0.0123P, \qquad P \lesssim 500 \tag{6}$$

$$\dot{M} = 6.07023\ 10^{-3}\frac{L}{cv_{\rm exp}}, \qquad P \gtrsim 500 \tag{7}$$

Here, $\dot{M}$ is given in units of $M_\odot\ {\rm yr}^{-1}$, the stellar luminosity L is expressed in $L_\odot$, the pulsation period P in days, c is the light speed (in km s^{-1}) and $v_{\rm exp}$ (in km s^{-1}) denotes the terminal velocity of stellar wind. In Eq. (7), $\dot{M}$ is the maximum mass loss rate which is obtained by equating the final mass momentum flux $\dot{M}v_{\rm exp}$ to the momentum flux of the entire stellar luminosity, according to the radiation-driven-wind theory (Castor et al. 1975). During calculation, at any time step, the mass-loss rate is chosen to be the minimum of the values given by Eq. (6) and (7).

The wind expansion velocity $v_{\rm exp}$ (in Km s^{-1}) is calculated in terms of the pulsation period P (in days):

$$v_{\rm exp} = -13.5 + 0.056P \tag{8}$$

with the additional constraint that $v_{\rm exp}$ lies in the range $3.0 - 15.0$ Km s^{-1}, the upper limit being the typical terminal velocity detected in high mass-loss rate OH/IR stars.

The pulsation period P is derived from the period-mass-radius relation (Eq. (4) in VW), with the assumption that variable AGB stars are pulsating in the fundamental mode:

$$\log P = -2.07 + 1.94\ \log R - 0.9\ \log M \tag{9}$$

where the period P is given in days; the stellar radius R and mass M are expressed in solar units.

We assume the TP-AGB phase to be complete either when the whole residual envelope has been ejected, or when the core mass has grown to the Chandrasekhar limit ($\sim 1.4 M_\odot$) just prior the carbon deflagration occurs. The latter condition is never met by our models, being prevented by the stripping action of stellar wind.

2.8. The third dredge-up

The third dredge-up has a crucial importance for the formation of carbon stars as it leads to ^{12}C surface enrichment. An analytical treatment of the process requires the knowledge of three basic inputs:

- the minimum core mass $M_{\rm c}^{\rm min}$;
- the efficiency λ;
- the chemical composition of the convective inter-shell.

A TP-AGB star can experience the third dredge-up when its core mass has grown over a critical value M_c^{min}, as indicated by detailed theoretical analysis (RV; Iben & Renzini 1983; BSc). The exact estimate of M_c^{min} is still a matter of debate. Among the several different prescriptions found in literature we recall $M_c^{min} \sim 0.6 M_\odot$ of RV, $M_c^{min} \sim 0.66 M_\odot$ of Lattanzio (1989c), $M_c^{min} = 0.58\ M_\odot$ in GdJ.

The free parameter λ expresses the dredge-up efficiency as it measures the extent of the inward penetration of the convective envelope. It is defined as the fraction of the core mass increment during the preceding interpulse period which is dredged up to the surface by envelope convection:

$$\lambda = \frac{\Delta M_{\rm dredge}}{\Delta M_{\rm c}} \tag{10}$$

The question on the real value of λ is also troublesome. On the one side numerical modelling of the third dredge-up estimate λ to be about $0.3 \div 0.4$ or even smaller (Iben & Renzini 1984; Lattanzio 1986; BSd); on the other side analytical models require a much higher value (e.g. $\lambda = 0.75$ in GdJ) in order to reproduce observational constraints (e.g. the luminosity function of carbon stars), a goal missed by the former approach.

Actually, both parameters M_c^{min} and λ significantly affect the predicted luminosity function of carbon stars, in particular the position of the peak and the low-luminosity tail of the distribution. In fact, lowering M_c^{min} favours the formation of carbon stars of lower mass and at the same time results in a longer carbon star phase; increasing λ corresponds to a relative increment of low mass stars which become carbon stars at lower luminosities (see GdJ for a detailed discussion).

Hence, the use of the parameters M_c^{min} and λ turns out to be relevant to analytical models of the TP-AGB phase. Their calibration based on observational constraints not only gives consistency to the theory, but it also offers a way to improve our understanding on the AGB stellar evolution. In this study we simply assume that both M_c^{min} and λ are constant, thus neglecting their dependence on metallicity, star mass, core mass, mixing length parameter. Though being a rough approximation, such a choice is to be intended in view of exploring the question of the third dredge-up so as to draw useful indications on the base of the observational information.

Indeed, the calibration of our TP-AGB model is based on the request of estimating these parameters so that the observed luminosity function of carbon stars in the LMC is reproduced (see Sect. 3.6). It is worth remarking that our subsequent nucleosynthetic analysis relies on this initial prescription. After several tests carried out with different values of M_c^{min} and λ, it results that the suitable ones are $M_c^{min} = 0.58\, M_\odot$ and $\lambda = 0.65$. These values are very close to those of GdJ, an agreement which may give a greater confidence to the theoretical results.

The material in the convective inter-shell after a thermal pulse and just before the penetration of the envelope is mainly formed by helium, carbon and oxygen. Traces of s-process elements may be also present. Detailed calculations of the inter-shell nucleosynthesis show that chemical abundances significantly depend on neither the core mass nor the metallicity (BSc). After the first few flashes, the inter-shell composition settles down to a constant mixture, with ^{12}C comprising 20% - 25% of the total mass, ^{16}O comprising $\sim$ 2% and ^{4}He comprising all the rest. In this study we adopt the following fixed abundances: 22% for ^{12}C produced by the triple alpha reaction and 2% for ^{16}O produced by the reaction $^{12}C(\alpha,\gamma)^{16}O$.

Actually, in order to estimate the effect of dredge-up on the surface abundances of all the 13 chemical elements we consider, we need to know the chemical composition of the inter-shell just before the onset of the flash (*pre-flash composition*) and that produced by helium-burning when the inter-shell convection is at its maximum extent, just prior the dredge-up phase (*post-flash composition*).

The *pre-flash composition* includes two different contributions corresponding to: i) material (with a mass $M_{\rm CNO}$) laid down by the H-burning shell during the previous interpulse period, in which most of the CNO abundance has been converted in ^{14}N and; ii) matter (with a mass $M_{\rm overlap}$) processed in the convective inter-shell during the preceding pulse.

Denoting by $M_{\rm CSH}$ the mass of the convective inter-shell, $\Delta M_{\rm c}$ the increment of the core mass during the previous interpulse period, then we get:

$$M_{\rm CNO} = \Delta M_{\rm c} \tag{11}$$

and

$$M_{\rm overlap} = M_{\rm CSH} - \Delta M_{\rm c} \tag{12}$$

where the mass (in $M_\odot$) of the convective inter-shell is expressed as a function of the current core mass $M_{\rm c}$, according to Iben (1977):

$$\log M_{\rm CSH} = -1.835 + 1.73 M_{\rm c} - 2.67 M_{\rm c}^2 \tag{13}$$

Hence, the fraction of matter in the current inter-shell which was once in the preceding one is $r = 1 - \Delta M_{\rm c}/M_{\rm CSH}$ (degree of overlap).

The adopted chemical composition of $M_{\rm CNO}$ is the following. The abundances (in mass fraction) of the 13 chemical elements are all negligible except for ^{4}He, ^{14}N, ^{20}Ne, ^{22}Ne, ^{25}Mg:

$$\begin{aligned} {}^{14}{\rm N} &= 14\, Y_{\rm CNO} \\ {}^{20}{\rm Ne} &= {}^{20}X^{\rm E} \\ {}^{22}{\rm Ne} &= {}^{22}X^{\rm E} \\ {}^{25}{\rm Mg} &= {}^{25}X^{\rm E} \\ {}^{4}{\rm He} &= 1 - {}^{14}X - {}^{20}X - {}^{22}X - {}^{25}X \end{aligned} \tag{14}$$

where the superscript E indicates the envelope abundance, and $Y_{\rm CNO} = \sum_j X_j^{\rm CNO}/A_j$ is the sum of the envelope abundances of all the CNO isotopes, each divided by the corresponding atomic weight A. The assumption of neglecting the abundances of the CNO isotopes (except for ^{14}N) will be justified below when comparing the effect produced on them by the subsequent He-shell flash.

Several theoretical analysis have been performed over the years to investigate the possible production of a small amount of primary ^{13}C near the H-discontinuity as the result of a suitable

mixing episode, following the pulse peak, that is able to carry protons down into the ^{12}C enriched region (Iben & Renzini 1984; Hollowell 1987; BSd; Hollowell & Iben 1988; Busso et al. 1992). When H-burning is reignited, a ^{13}C-pocket is naturally produced.

When a thermal pulse develops, besides the dominant production of ^{12}C and ^{16}O, other important nucleosynthetic processes (α capture reactions) can take place in the convective inter-shell.

- Freshly produced ^{14}N is almost completely converted into ^{22}Ne via the chain ^{14}N(α, γ) ^{18}F(β^+, ν) ^{18}O(α, γ) ^{22}Ne (BSc).
- A certain amount of ^{22}Ne may burn via the neutron source reaction ^{22}Ne(α, n)^{25}Mg. The extent of the nuclear conversion depends strongly on M_c, being of about 1% for $M_c \lesssim 0.7$ $M_\odot$, and being nearly complete for $M_c \geq 1$ $M_\odot$ (Gallino et al. 1988).
- When the inter-shell convection extends upward and and engulfs the ^{13}C-pocket previously produced, this can be easily burnt via the neutron source reaction ^{13}C(α, γ)^{16}O (Busso et al.1992). Recently, Straniero et al. (1995) have shown that the ingestion of the ^{13}C-pocket may be totally prevented by the radiative ^{13}C burning during the interpulse period.

Since in our models the core mass never grows above 1 $M_\odot$, the conversion ^{22}Ne(α, n)^{25}Mg is assumed to have a very low efficiency (1%). Hence, the adopted *post-flash composition* of the convective inter-shell is given below, where the abundance (in mass fraction) of each chemical element is specified. We denote the pre-flash chemical abundances by a superscript preF.

$$
\begin{aligned}
&H = 0\\
&^3\mathrm{He} = 0\\
&^{12}\mathrm{C} = 0.22\\
&^{13}\mathrm{C} = 0\\
&^{14}\mathrm{N} = 0\\
&^{15}\mathrm{N} = 0\\
&^{16}\mathrm{O} = 0.02\\
&^{17}\mathrm{O} = 0\\
&^{18}\mathrm{O} = 0\\
&^{20}\mathrm{Ne} = {}^{20}\mathrm{Ne}^{\mathrm{preF}}\\
&^{22}\mathrm{Ne} = {}^{22}\mathrm{Ne}^{\mathrm{preF}} + 0.99 \times 22 \times {}^{14}\mathrm{N}^{\mathrm{preF}}/14\\
&^{25}\mathrm{Mg} = {}^{25}\mathrm{Mg}^{\mathrm{preF}} + 0.01 \times 25 \times {}^{14}\mathrm{N}^{\mathrm{preF}}/14\\
&^4\mathrm{He} = 1 - (\text{the sum of all the other abundances})
\end{aligned}
\tag{15}
$$

It is found that primary production of ^{12}C, ^{16}O is predominant over the corresponding secondary abundances left by the H-burning shell during the preceding interpulse period, so that neglecting them in the *pre-flash composition* seems reasonable. The *post-flash* abundances of all the other CNO isotopes are assumed zero on the base of the following considerations.

The ^{13}C-pocket is totally burnt via the reaction ^{13}C(α, γ)^{16}O, in both the convective and radiative cases. The conversion of ^{14}N into ^{18}O and then into ^{22}Ne is complete, as already referred above. The residual abundance of ^{15}N expected from the CNO cycle is extremely small (e.g. equilibrium ratio ^{15}N/^{14}N $\sim 4 \times 10^{-5}$ at all temperatures), and then it can be neglected (Clayton 1983). From comparing the nuclear reaction rates at the typical inter-shell temperature during a pulse ($\sim 2.5 - 3 \times 10^8$ K), it turns out that ^{17}O is rapidly destroyed via the reactions (e.g. ^{17}O(α, γ)^{21}Ne and ^{17}O(α, n)^{20}Ne). In fact, the rates of alpha capture on ^{17}O are typically 2 o 3 order of magnitude faster than that of the efficient triple alpha reaction (Caughlan & Fowler 1988).

At those temperatures, also ^{3}He is expected to be quickly destroyed by interactions with itself and with ^{4}He, while almost no ^{20}Ne can be synthesized as a result of ^{16}O(α, γ)^{20}Ne because of the long ^{16}O lifetime, so that its abundance is nearly unchanged.

Denoting by X_i^{old}, X_i^{CSH}, M_{env} the abundance of the element i in the envelope, in the convective inter-shell and the mass of the envelope just before the dredge-up event, respectively, the new surface abundance X_i^{new} as it results after the mixing episode is:

$$
X_i^{\mathrm{new}} = \frac{X_i^{\mathrm{old}} M_{\mathrm{env}} + X_i^{\mathrm{CSH}} \Delta M_{\mathrm{dredge}}}{M_{\mathrm{env}} + \Delta M_{\mathrm{dredge}}} \tag{16}
$$

Finally, after any dredge-up event, the core mass is reduced by $\Delta M_{\mathrm{dredge}}$ and the envelope mass is increased by the same amount.

2.9. The effective temperature

The effective temperature T_{eff} of a TP-AGB star is derived from the numerical integration of a complete envelope model, the same one used in the evolutionary code of Padua. The value of T_{eff} is determined by imposing the condition $M_{\mathrm{CE}}(T_{\mathrm{eff}}) = M_c$, meaning that the mass coordinate M_{CE} of the base of the convective envelope must coincide with the core mass M_c. In fact, complete evolutionary analysis show that during most of the interpulse phase the deepest layers of the envelope lie very close in mass to the hydrogen-burning shell. In general, during the quiescent regime the difference $M_{\mathrm{CE}} - M_c$ keeps within a few times 10^{-5} $M_\odot$ (BSd).

During calculation, at each time step, for specified values of the total mass M, core mass M_c, total luminosity L an iterative procedure is carried out in order to fulfil the above condition (with a relative accuracy $\epsilon = 10^{-5}$).

We use the value of the mixing length parameter $\alpha = 1.63$ ($\alpha = l/H_P$ in the standard notation), a value derived from the calibration of the solar model (Bressan et al. 1993) and adopted for computing the evolutionary tracks from which we extract the initial conditions of our TP-AGB models (see Sect. 2.1). It is worth remarking that the base of the convective envelope sits in a zone just outside the core which is very thin in mass, but where the temperature gradient is extremely steep. The investigation of BSd shows that the value of α has a relatively small effect on the depth in mass of AGB star convective envelope, while it produces a large effect on the temperature stratification along the envelope.

2.10. Envelope burning

Once the density $\rho(r)$ and temperature $T(r)$ structures along the radial coordinate r of the envelope are known, a detailed quantitative treatment of nucleosynthesis in the envelope is performed. The envelope is divided into a number of concentric shells, each corresponding to local mean values of ρ and T. The adopted criterium is that of getting a smooth discrete sequence of temperature ($\Delta \log \sim 0.01$ from shell to shell). The network of the nuclear reactions involved is the following:

$$
\begin{array}{l}
^{12}\mathrm{C} + {}^{1}\mathrm{H} \longrightarrow {}^{13}\mathrm{C} + \gamma + \beta^{+} + \nu \\
^{13}\mathrm{C} + {}^{1}\mathrm{H} \longrightarrow {}^{14}\mathrm{N} + \gamma \\
^{14}\mathrm{N} + {}^{1}\mathrm{H} \longrightarrow {}^{15}\mathrm{N} + \gamma + \beta^{+} + \nu \\
^{15}\mathrm{N} + {}^{1}\mathrm{H} \longrightarrow {}^{4}\mathrm{He} + {}^{12}\mathrm{C} \\
^{15}\mathrm{N} + {}^{1}\mathrm{H} \longrightarrow {}^{16}\mathrm{O} + \gamma \\
^{16}\mathrm{O} + {}^{1}\mathrm{H} \longrightarrow {}^{17}\mathrm{O} + \gamma + \beta^{+} + \nu \\
^{17}\mathrm{O} + {}^{1}\mathrm{H} \longrightarrow {}^{4}\mathrm{He} + {}^{14}\mathrm{N} \\
^{17}\mathrm{O} + {}^{1}\mathrm{H} \longrightarrow {}^{18}\mathrm{O} + \gamma + \beta^{+} + \nu \\
^{18}\mathrm{O} + {}^{1}\mathrm{H} \longrightarrow {}^{4}\mathrm{He} + {}^{15}\mathrm{N} \\
^{18}\mathrm{O} + {}^{1}\mathrm{H} \longrightarrow {}^{19}\mathrm{F} + \gamma \\
^{19}\mathrm{F} + {}^{1}\mathrm{H} \longrightarrow {}^{4}\mathrm{He} + {}^{16}\mathrm{O}
\end{array}
\qquad (17)
$$

Nuclear rates and Q-values are those of Caughlan & Fowler (1988). In particular, we adopt the value 0.1 for the factor f included in the analytic expressions of the nuclear rates corresponding to the reactions $^{15}\mathrm{N}(p,\alpha)^{12}\mathrm{C}$, $^{17}\mathrm{O}(p,\alpha)^{14}\mathrm{N}$, $^{17}\mathrm{O}(p,\gamma)^{18}\mathrm{F}$. The screening factors are derived from Graboske et al. (1973). The β-decay processes are considered to take place instantaneously.

In general, the evaluation of time changes in the chemical abundances due to nuclear reactions requires the integration of the system of equations below:

$$
\frac{d}{dt} Y_i = -[ij]\ Y_i Y_j + [rs]\ Y_r Y_s, \qquad i = 1, \ldots N_{\mathrm{el}} \qquad (18)
$$

where $Y_i = X_i/A_i$, X_i, and A_i denote the abundance by number (in mole g^{-1}), the abundance by mass, and the atomic mass of the elemental species i, respectively. In the right-hand side of Eq. (18), $[ij]$ stands for the rate of the generic reaction which converts the element i into another nucleus because of the interaction with the element j, whereas $[rs]$ is the rate of the generic reaction transforming nuclei s and r into the element i.

Instead of adopting the implicit matrix method (widely described in Clayton 1983) we choose an explicit method based on the comparison between two characteristic timescales :

- the nuclear lifetime against a proton capture τ_{N};
- the convective lifetime τ_{conv}

The former timescale is calculated for each chemical species and in every envelope shell. The latter timescale defines the time that an average convective eddy, with a speed v_{conv}, takes to move throughout the radial extension Δr of a given shell in the envelope:

$$
\tau_{\mathrm{conv}} = \frac{\Delta r}{v_{\mathrm{conv}}} \qquad (19)
$$

To estimate v_{conv} we refer to the standard theory of convection under the assumption of a fully ionized perfect gas (Cox & Giuli 1968, chapter XIV). At every fixed instant t and for each shell in the envelope, before solving the system, we calculate τ_{N} for all chemical species involved in nuclear reactions, and the timescale τ_{conv}. Denoting by Y_i^{old} the envelope abundance of a given chemical element i at the time t, then its new envelope abundance Y_i^{new} at the time $t + \Delta t$ is derived by applying the following criterium:

If $\tau_{\mathrm{N}} > \tau_{\mathrm{conv}}$ all over the envelope, then the effect of convective mixing prevails over nuclear consumption so that no drastic changes can occur. The corresponding Eq. (18) is converted into an explicit finite difference equation and the new abundance Y_i^{new} is obtained from the mass average of all the local chemical variations:

$$
Y_i^{\mathrm{new}} = Y_i^{\mathrm{old}} + \frac{1}{M_{\mathrm{env}}} \sum_{k=1}^{N_{\mathrm{shell}}} \Delta Y_{ik} M_k^{\mathrm{shell}} \qquad (20)
$$

The summation is performed over the total number N_{shell} of the shells, M_k^{shell} is the mass of the shell k, ΔY_{ik} is the abundance variation of the element i produced by nuclear reactions in the shell k, and M_{env} is the mass of the envelope.

If $\tau_{\mathrm{N}} < \tau_{\mathrm{conv}}$ then the element achieves its equilibrium abundance according to the local thermodynamical conditions, before leaving the shell. In our study this happens only for few species ($^{15}\mathrm{N}$, $^{18}\mathrm{O}$, $^{13}\mathrm{C}$, $^{12}\mathrm{C}$) and it is limited to the case of the 4 $M_{\odot}$ $Z = 0.008$ model, inside a very thin region deep in the envelope whose mass does not exceed a few times $10^{-5} M_{\odot}$ (see Figs. 5 and 6) (equilibrium region of a given element).

Given the extremely steep temperature gradient it is reasonable to assume that in the matter flowing away from this region, the above elements keep the equilibrium abundances they attained inside the outermost shell where the condition $\tau_{\mathrm{N}} < \tau_{\mathrm{conv}}$ is met (transition shell).

We evaluate the mass that leaves the equilibrium region as $\Delta M^{\mathrm{E}} = 1/2 \times 4\pi R_{\mathrm{tr}}^2 \rho(R_{\mathrm{tr}}) v_{\mathrm{conv}}(R_{\mathrm{tr}}) dt$, where all the quantities are computed at the transition shell, and the factor 1/2 arises from the mass conservation in a convective region.

Thus, the new envelope abundance will result from the average contribution of the equilibrium region, the flow of matter with equilibrium abundance of the transition shell, and the unprocessed material.

The first contribution is negligible because of the tiny size of the equilibrium region and the new envelope abundance Y_i^{new} of the element i at the time $t + \Delta t$ is given by:

$$
Y_i^{\mathrm{new}} = \frac{Y_i^{\mathrm{E}} \Delta M^{\mathrm{E}} + Y_i^{\mathrm{old}} (M_{\mathrm{env}} - \Delta M^{\mathrm{E}})}{M_{\mathrm{env}}} \qquad (21)
$$

It is clear that the radial width of the shells is critical because it affects the value of τ_{conv}. However if $\tau_{\mathrm{N}} < \tau_{\mathrm{conv}}$ in a shell of a given size, then the element will approach the equilibrium abundance for whatever subdivision of the layer because, on the average, the whole time spent by the convective eddy inside that shell has been physically tested to be longer than the mean nuclear lifetime of the element. On the other hand, the maximum

Table 1. Initial conditions at the first thermal pulse for $Z = 0.02$: M is the total mass in $M_\odot$, M_c is the core mass in $M_\odot$, L is the logarithm of the luminosity in $L_\odot$, $T_{\rm eff}$ is the logarithm of the effective temperature.

M	M_c	L	$T_{\rm eff}$
0.7	0.544	3.339	3.462
0.8	0.546	3.350	3.463
0.9	0.545	3.322	3.475
1.0	0.547	3.325	3.482
1.2	0.554	3.369	3.489
1.3	0.562	3.419	3.488
1.4	0.557	3.400	3.499
1.5	0.562	3.422	3.503
1.6	0.557	3.392	3.512
1.8	0.546	3.335	3.529
2.0	0.560	3.430	3.525
2.5	0.568	3.459	3.549
3.0	0.627	3.702	3.535
4.0	0.745	4.188	3.494

Table 2. The same as in Table 1, but with $Z = 0.008$

M	M_c	L	$T_{\rm eff}$
0.6	0.528	3.167	3.547
0.68	0.535	3.200	3.529
0.75	0.538	3.232	3.525
0.9	0.541	3.242	3.537
1.1	0.548	3.283	3.545
1.2	0.550	3.295	3.547
1.3	0.552	3.295	3.555
1.5	0.554	3.299	3.563
1.8	0.546	3.280	3.578
2.0	0.533	3.217	3.591
2.5	0.577	3.429	3.587
3.0	0.653	3.699	3.572
4.0	0.805	4.239	3.537

size allowed to the shells is fixed by the criterium of getting a smooth temperature stratification, permitting the definition of meaningful average quantities.

Actually, the real situation is more complex than this simple description. Convective motions produce a continue spatial redistribution of the material in the envelope, thus affecting the products of nuclear reactions for their extreme sensitivity to local values of temperature and density. Hence to proceed correctly a convective diffusion algorithm should be used (Sackmann & Boothroyd 1992).

3. Results

We calculate the semi-analytical TP-AGB evolution for two different values of metallicity ($Z = 0.02$, $Y = 0.28$; and $Z = 0.008$, $Y = 0.25$), each set of tracks covering the mass range $0.7 M_\odot \lesssim M \leq 4 M_\odot$ (main sequence values).

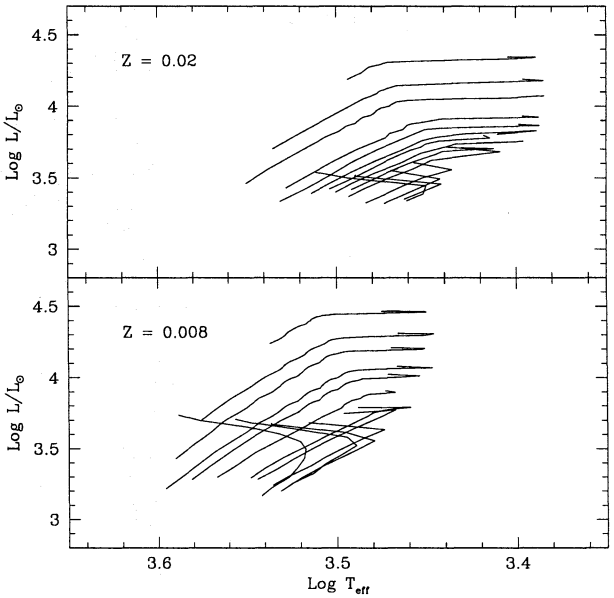

Fig. 1. TP-AGB evolutionary tracks in the H-R Diagram.

The initial conditions at the first significant flash are tabulated in Tables 1 and 2. Fig. 1 shows the predicted TP-AGB evolution in the H-R Diagram for both sets of tracks.

3.1. Nucleosynthesis

We now discuss the possible changes in the surface chemical composition caused by dredge-up episodes and/or nucleosynthetic processes in the deepest layers of the envelope (envelope burning).

Very low-mass stars do not experience any variation of the elemental abundances because they end their AGB evolution before their core mass has grown over the minimum value $M_c^{\rm min}$ for the third dredge-up to occur. With our choice $M_c^{\rm min} = 0.58\, M_\odot$, the corresponding lower limit of the main sequence mass turns out to be around $1.3 M_\odot$ for $Z = 0.02$ and $1.1 M_\odot$ for $Z = 0.008$.

Fig. 2 shows the evolution of a few chemical abundance ratios in the envelope for the model $M = 2.5 M_\odot$, $Z = 0.008$. The changes of the surface chemical ratios reflect the effect of the third dredge-up which is the only mechanism able to alter the surface composition of this star model. The dominant result is the ^{12}C enrichment which causes the ratios ^{12}C/^{13}C, C/O, C/N to increase, while the contribution of the dredged-up oxygen turns down the N/O ratio.

A critical main sequence mass $M_{\rm EB}^{\rm min}$ also exists for envelope burning to operate: in lower mass stars the temperature at the base of the convective envelope, $T_{\rm B}$, never reaches values high enough for significant CNO processing to occur ($T_{\rm B} \geq 40 \times 10^6$ K). The estimate of $M_{\rm EB}^{\rm min}$ is found to be strongly dependent on the metal content in the envelope and the adopted mixing length

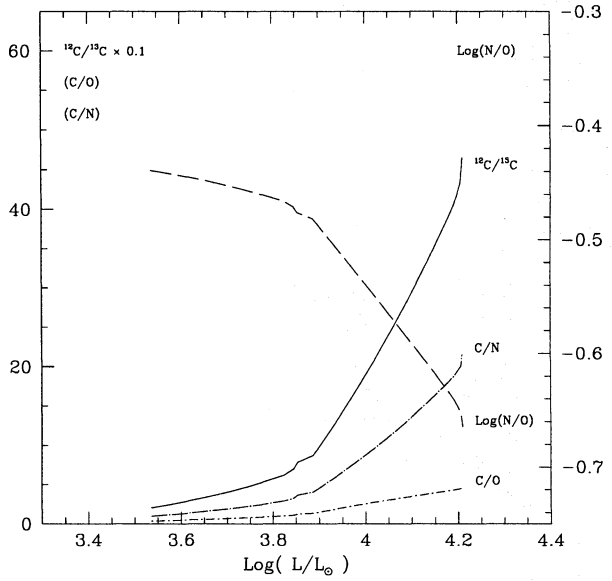

Fig. 2. $^{12}C/^{13}C$, C/O, C/N and log(N/O) (right scale) vs. luminosity for an evolving TP-AGB star of $2.5M_\odot$, $Z = 0.008$. The lines connect the values of chemical ratios evaluated at the pre-flash luminosity maximum preceding each pulse.

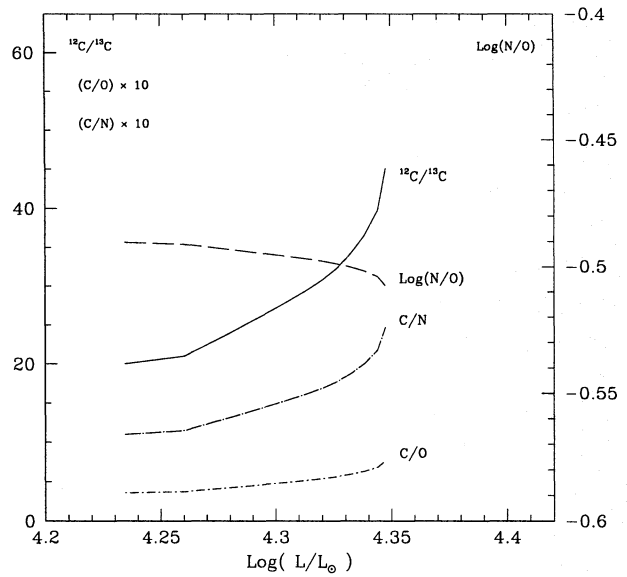

Fig. 3. The same as in Fig. 2, except for $4M_\odot$, $Z = 0.02$.

parameter α (Sect. 3.1.1). The question of the overluminosity produced by envelope burning is discussed below in Sect. 3.1.2.

A larger metallicity produces lower values of T_B. In fact, we derive $M_{EB}^{min} \sim 4M_\odot$ for the case $Z = 0.008$, while at the same mass but with $Z = 0.02$ our model is just lightly affected by envelope burning. This is well illustrated in Figs. 3 and 4.

In Fig. 3 the trend of the chemical ratios for the ($M/M_\odot = 4$, $Z = 0.02$) model essentially reflects the chemical enrichment due to dredge-up, similarly to Fig. 2. The case ($M/M_\odot = 4$, $Z = 0.008$) appears to be largely different because of envelope burning. The effect is clear from Fig. 4. Initially, $^{12}C/^{13}C$, C/O, C/N are expected to increase thanks to the dredge-up events, but when envelope burning becomes effective ($T_B \geq 40 \times 10^6$ K), ^{12}C is quickly converted into ^{13}C via the first reactions of the CN cycle. Hence, the $^{12}C/^{13}C$ ratio, after reaching a maximum, begins to decline. At this stage, the nuclear production of ^{14}N remains marginal, so that the C/N ratio is still increasing.

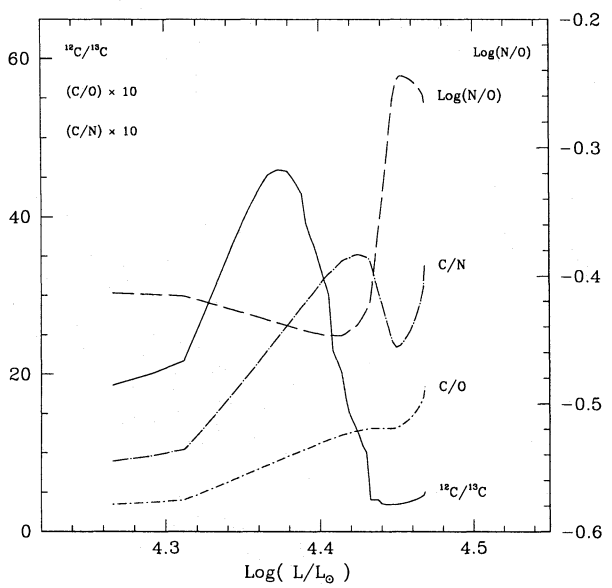

Fig. 4. The same as in Fig. 2, except for $4M_\odot$, $Z = 0.008$.

As soon as carbon isotopes ^{12}C and ^{13}C meet their equilibrium condition, the nuclear conversion into ^{14}N becomes efficient, causing the C/N ratio to diminish and the N/O ratio to rise. Finally, when a substantial fraction of the envelope has been ejected, the declining temperature in the deepest layers of the envelope significantly weakens the efficiency of the nuclear reactions. The effect of the third dredge-up becomes dominant again and produces a brief increasing of the $^{12}C/^{13}C$, C/O, C/N ratios.

In Table 3 there are shown the expected isotope ratios C/O, $^{12}C/^{13}C$, $^{20}Ne/^{22}Ne$ for some AGB star models for both metallicities. For each mass the data refer to three precise evolutionary stages: 1) the starting of the TP-AGB; 2) the transition to carbon star (when present); 3) the end of the TP-AGB evolution. Concerning the transition from the M-phase (C/O $\leq$ 1) to the C-phase (C/O $\geq$ 1), we find that the model ($4M_\odot$, $Z = 0.02$) does not become a carbon star and reaches a maximum value C/O $\sim$ 0.7, while the model ($4M_\odot$, $Z = 0.008$) makes the transition relatively early in the evolution with a final value C/O $\sim$ 2.

The interpretation of such strong differences between the 4 $M_\odot$ models of different metallicities may be ascribed to the combined effect of the following causes:

– Lower metallicities favour the production of carbon stars. In fact, as the original envelope abundances of carbon and oxygen are smaller than in metal-rich stars, for a same fixed quantity of dredged-up carbon, metal-poor stars attain a

Table 3. Expected isotopic ratios from AGB stars at different evolutionary stages. M is the mass at the first thermal pulse; log L is the stellar luminosity (in $L_\odot$). See text for further explanation.

M	log$L$	C/O	$^{12}C/^{13}C$	$^{20}Ne/^{22}Ne$
	$Z = 0.02$			
1.5	3.42	0.356	22.090	7.446
	3.80	0.991	65.394	1.584
2.5	3.46	0.344	20.399	7.446
	4.00	1.051	66.750	1.195
	4.07	1.516	100.958	0.657
4.0	4.19	0.355	20.017	7.446
	4.35	0.767	45.055	1.983
	$Z = 0.008$			
1.5	3.30	0.352	22.909	7.444
	3.84	1.089	77.808	2.335
	3.93	2.283	295.328	0.384
2.5	3.43	0.338	20.091	7.444
	3.85	1.095	69.944	0.520
	4.21	4.658	464.857	0.142
4.0	4.23	0.344	18.604	7.444
	4.39	1.008	44.134	2.523
	4.47	1.843	4.665	0.928

greater increment of the surface C/O ratio if compared to the high-metallicity case.
Moreover, since the overall duration of the TP-AGB evolution is expected to be longer for lower metallicities (see Sect. 3.4), stars may suffer a greater number of thermal pulses and thus the surface enrichment of ^{12}C is favoured.

– Envelope burning operates more efficiently in metal-poor stars because of the higher temperature at the base of the convective envelope.

3.1.1. The sensitivity of the results to α

The crucial dependence of envelope burning on the mixing-length parameter α is well shown by Boothroyd et al.(1993). To investigate the effect of varying α on the temperature structure along the convective envelope, we perform a simple experiment on our model of 4 $M_\odot$ calculated at $Z = 0.008$. We refer to the evolutionary stage at the end of the 35th interpulse period, with a current mass $M = 3.947 M_\odot$, a core mass $M_c = 0.839 M_\odot$, a luminosity log $L/L_\odot = 4.414$.

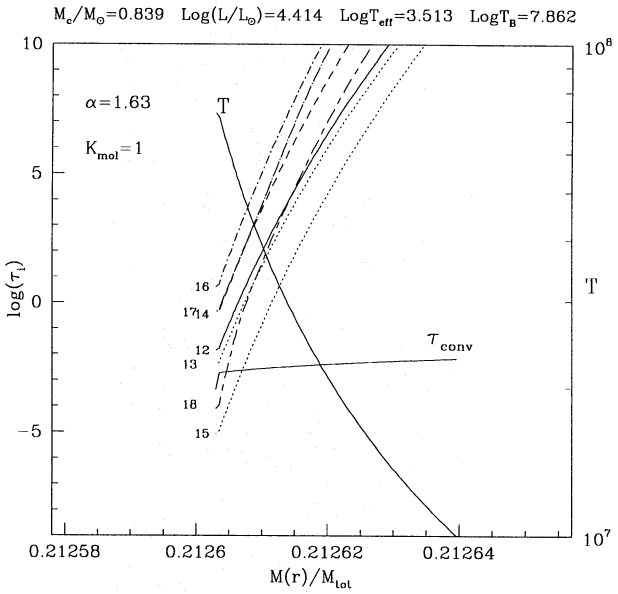

Fig. 5. Nuclear lifetimes τ_i (in years) against neutron captures of a few CNO isotopes (^{12}C, ^{13}C, ^{14}N, ^{15}N, ^{16}O, ^{17}O, ^{18}O, each τ_i denoted by its atomic number) and the temperature (right logarithmic scale) as functions of the mass faction of the deepest layers down to the base of the envelope. $M(r)/M_{tot}$ is the fraction of the total mass M_{tot} of the star which is inside a sphere of radius r.

The integration of the envelope model with $\alpha = 1.63$ gives a value of the effective temperature log $T_{eff} = 3.513$ and a temperature at the base of the convective envelope log $T_B = 7.862$. Increasing α to a value 2.5 (while keeping constant all the other variables) results in getting both the effective temperature (log $T_{eff} = 3.590$) and the temperature T_B (log $T_B = 8.026$) hotter.

Actually, a free variation of α does not allow to discern its effect on the internal structure (e.g. the temperature structure along the envelope) from that which is possibly due to a change of the surface conditions (e.g. the effective temperature and hence the stellar radius). Moreover, in practice, with regard to the calculation of stellar models, the adoption of a new value of α is always required every time any physical input is updated. The theoretical purpose is to reproduce observational constraints, such as the luminosity and the effective temperature of the Sun by the corresponding solar model, and the morphology of the red giant branches in the color-magnitude diagrams of observed stellar clusters.

Hence, we increment the molecular opacities (by a multiplicative factor $K_{mol} = 6.982$) in order to relocate the model calculated with $\alpha = 2.5$ at the same position in the H-R Diagram corresponding to the model calculated with $\alpha = 1.63$ (e.g. with the same effective temperature and luminosity). In this way, we just simulate a possible change in the physical inputs of the envelope model (e.g. a hypothetical revision of the molecular opacities) and the subsequent necessary recalibration of α. The temperature at the base of the convective envelope results log $T_B = 7.925$.

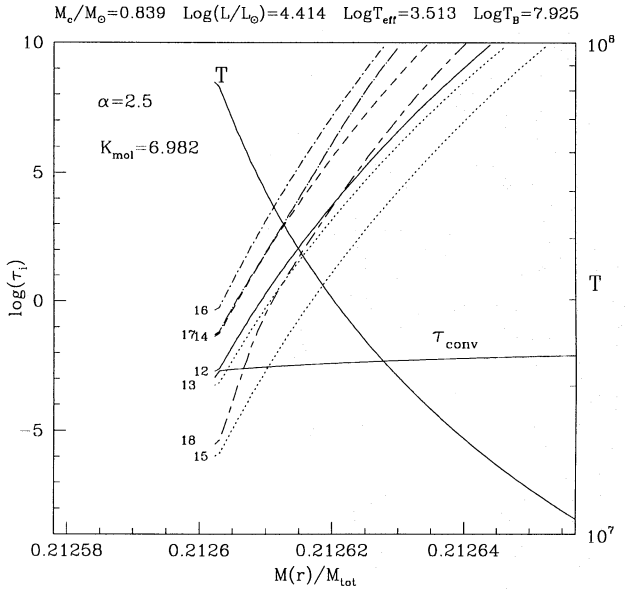

Fig. 6. The same as in Fig. 5, except for α = 2.5 and with molecular opacities multiplied by a factor $K_{\rm mol}$ = 6.982.

From the comparison between the two envelope models (α = 1.63, $K_{\rm mol}$ = 1) and (α = 2.5, $K_{\rm mol}$ = 6.982) a significant difference emerges (see Figs. 5 and 6): the latter case corresponds to an increase of the local temperature and to a larger region where the temperature is above 10^7 K. Both factors contribute to a more efficient CNO burning.

Hence, this confirms that different recalibrations of the parameter α, which follow any major variation of the input physics, while providing the same surface conditions, do produce different equilibrium configurations of the interior structure.

3.1.2. Limitation of the model to an excess of luminosity

At each time step, the integration of the envelope model is carried out with the assumption that the stellar luminosity is constant and that no luminosity gradient exists along the radial extension of the envelope. That is equivalent to exclude any active energy source inside the envelope.

However, nuclear burning at the base of the convective envelope is an energy source, so that the above assumption is not fully correct and the model may lose validity. Indeed, the excess of luminosity $L_{\rm CNO}$ produced by envelope burning can make the star deviate significantly from the canonical $M_{\rm c} - L$ relation (Blöcker & Schönberner 1991; Blöcker 1995) to a luminosity much higher than otherwise predicted at a given core mass (e.g. a factor 3 for the 7 $M_\odot$ model).

Investigating the impact of a luminosity excess on our model we find a consequent local increase of the temperature in the envelope. This circumstance would yield more efficient nuclear burning, so that a further increment in luminosity is expected. Moreover, the resulting gradient in luminosity would affect the radiative gradient in temperature at the base of the convective envelope. Thus, both the assumptions of the constancy of the luminosity and that of the base of envelope just extending down to the core are not strictly correct.

Nevertheless, our calculations indicate that the temperature stratification is not significantly altered by envelope burning if its luminosity contribution is as much as few percents of the total stellar luminosity and thus, in this circumstance, our assumptions are acceptable and the validity of the model not compromised.

The inclusion of an equation correctly describing the luminosity gradient along the envelope is postponed to a future study. At this stage we just evaluate, for each stellar mass, the relative contribution of envelope burning to the total luminosity. We find that only in the 4 $M_\odot$, Z = 0.008 model is $L_{\rm CNO}$ much greater than the stellar luminosity mostly generated by the H-burning shell ($L_{\rm CNO}/L \sim 80$ % at maximum), while in all the other models it is always indeed negligible.

3.2. Stellar yields

We evaluate the contribution of low and intermediate-mass stars to the chemical enrichment of the interstellar medium (ISM). To this aim, we calculate, for each given chemical species i, the corresponding stellar yield $M_{\rm y}(i)$ (RV), usually defined as the mass of the element which is synthesized by a star and returned to the ISM during its entire life.

Before the TP-AGB phase, the chemical composition of the envelope may change with respect to its main sequence value because of the occurrence of dredge-up events, namely:

1. The first dredge-up.
   This process operates as a star becomes a red giant for the first time and corresponds to the penetration of the convective envelope into regions which have already experienced partial CNO-burning, so that newly synthesized material is dredged-up to the surface and mixed throughout the envelope. The most important effect is the decrease of ^{12}C surface abundance, and the enhancement of those of ^{13}C and ^{14}N.
2. The second dredge-up.
   Complete evolutionary models predict that stars more massive than $\sim 3 - 5 M_\odot$ (depending on metallicity) experience a second episode of surface chemical variation during the initial evolution along the E-AGB phase. Soon after the hydrogen-burning shell extinguishes, the base of the convective envelope once again deepens in the interior and newly processed chemical elements are brought to the surface. In the dredged-up material the CNO cycle has produced the complete conversion of H into ^{4}He and ^{12}C and ^{13}C have been transformed into ^{14}N. The abundances of ^{4}He and ^{14}N are expected to increase, while those of ^{12}C, ^{13}C and ^{16}O decrease.

We need to include the contribution to $M_{\rm y}(i)$ coming from the evolutionary stages previous to the TP-AGB phase, that is essentially the ejection by stellar wind of newly processed material during the ascent of the Red Giant Branch (RGB). To account for the changes in the surface chemical composition caused by the first and second dredge-up episodes, we use the

Table 4. Stellar yields $M_y(i)$ of low and intermediate mass stars with initial metallicity $Z = 0.02$, calculated with $M_c^{min} = 0.58 M_\odot$, $\lambda = 0.65$. The initial mass M_i and the total amount of ejected material M_{ej} are indicated (in $M_\odot$).

M_i	M_{ej}	$M_y(^3He)$	$M_y(^4He)$	$M_y(^{12}C)$	$M_y(^{13}C)$	$M_y(^{14}N)$	$M_y(^{15}N)$
0.915	0.356	7.200E-04	5.626E-03	-7.754E-05	2.165E-05	6.718E-05	-2.414E-07
0.987	0.429	7.544E-04	6.953E-03	-1.206E-04	3.170E-05	1.065E-04	-3.404E-07
1.066	0.504	7.415E-04	8.315E-03	-1.986E-04	4.190E-05	1.866E-04	-4.753E-07
1.147	0.579	7.046E-04	9.410E-03	-3.029E-04	5.138E-05	2.987E-04	-6.378E-07
1.318	0.737	6.305E-04	1.065E-02	-5.687E-04	7.648E-05	5.827E-04	-1.047E-06
1.492	0.907	5.947E-04	1.249E-02	-4.071E-04	1.026E-04	9.838E-04	-1.584E-06
1.579	0.988	5.556E-04	1.900E-02	2.192E-03	1.073E-04	1.211E-03	-1.860E-06
1.665	1.074	5.190E-04	1.742E-02	1.001E-03	1.191E-04	1.386E-03	-2.110E-06
1.837	1.250	4.601E-04	2.106E-02	7.029E-04	1.355E-04	1.817E-03	-2.566E-06
2.000	1.396	3.960E-04	3.699E-02	5.486E-03	1.496E-04	2.173E-03	-3.050E-06
2.500	1.863	4.888E-03	7.916E-02	1.648E-02	1.892E-04	3.336E-03	-4.343E-06
3.000	2.339	2.366E-04	7.502E-02	5.607E-03	2.459E-04	4.770E-03	-5.368E-06
4.000	3.231	1.611E-04	8.401E-02	2.698E-03	3.718E-04	6.263E-03	-7.190E-06

M_i	M_{ej}	$M_y(^{16}O)$	$M_y(^{17}O)$	$M_y(^{18}O)$	$M_y(^{20}Ne)$	$M_y(^{22}Ne)$	$M_y(^{25}Mg)$
0.915	0.356	0	4.776E-09	-9.107E-08	0	0	0
0.987	0.429	0	1.129E-08	-1.637E-07	0	0	0
1.066	0.504	0	2.867E-08	-3.007E-07	0	0	0
1.147	0.579	0	7.073E-08	-5.726E-07	0	0	0
1.318	0.737	0	3.803E-07	-1.351E-06	0	0	0
1.492	0.907	1.964E-05	1.146E-06	-2.531E-06	0	6.280E-05	6.874E-07
1.579	0.988	1.416E-04	4.645E-06	-3.698E-06	0	2.938E-04	1.113E-06
1.665	1.074	6.400E-05	3.074E-05	-4.209E-06	0	2.791E-04	3.183E-06
1.837	1.250	-7.506E-05	1.121E-04	-5.450E-06	0	2.836E-04	3.191E-06
2.000	1.396	-5.554E-05	2.022E-04	-6.930E-06	0	9.852E-04	1.127E-05
2.500	1.863	-1.501E-04	3.839E-04	-1.092E-05	0	3.049E-03	3.487E-05
3.000	2.339	-1.148E-03	4.953E-04	-1.293E-05	0	1.207E-03	1.379E-05
4.000	3.231	-1.691E-03	4.342E-04	-1.522E-05	0	9.186E-04	1.047E-05

results of the complete evolutionary models calculated by Bressan et al. (1993) for $Z = 0.02$ and by Fagotto et al. (1994) for $Z = 0.008$ (see Sect. 2.1).

Denoting by $X^0(i)$, $X^1(i)$, $X^j(i)$, respectively, the abundance of the species i on the ZAMS, after the first dredge-up and after the j^{th} dredge-up event along the AGB phase, we get:

$$M_y(i) = M_y(i)_{RGB} + M_y(i)_{AGB} \tag{22}$$

where

$$M_y(i)_{RGB} = [X^1(i) - X^0(i)]\Delta M^{ej}_{RGB} \tag{23}$$

and

$$M_y(i)_{AGB} = \sum_j [X^j(i) - X^0(i)]\Delta M^{ej}_{j,AGB} \tag{24}$$

In Eq. (23) ΔM^{ej}_{RGB} is the mass of the envelope ejected during the entire RGB phase. It is calculated by means of the Reimers prescription (Reimers 1975) for the mass-loss rate ($\dot{M} = \eta RLM^{-1}$) to the complete evolutionary tracks (calculated at constant mass) referenced above. A coefficient $\eta = 0.35$ is adopted to fulfil the classical observational constraint that indicates $\sim 0.2\ M_\odot$ the typical mass ejected by HB stars in globular clusters during the previous RGB phase (Renzini & Fusi Pecci 1988). We verify that only low-mass stars – those which experience He-flash at the RGB tip – loose a considerable amount of matter along RGB. At larger masses ($M \geq M_{HeF}$ with $M_{HeF} \sim 1.8 - 2.2\ M_\odot$, depending on metallicity) ΔM^{ej}_{RGB} can be neglected.

In Eq. (24) $M^{ej}_{j,AGB}$ is the mass ejected during the j^{th} thermal pulse and the subsequent interpulse period, and $M_y(i)_{AGB}$ is calculated just summing all the partial contributions from every dredge-up event during the AGB evolution. It is worth noting that, with the adopted prescription for $\dot{M}$ (Sect. 2.7), the total stellar mass remains essentially unchanged during the

Table 5. The same as in Table 4, except for $Z = 0.008$.

M_i	M_{ej}	$M_y(^3He)$	$M_y(^4He)$	$M_y(^{12}C)$	$M_y(^{13}C)$	$M_y(^{14}N)$	$M_y(^{15}N)$
0.819	0.241	5.260E-04	3.526E-03	-1.490E-05	5.905E-06	1.154E-05	-6.048E-08
0.877	0.300	6.319E-04	4.544E-03	-2.203E-05	7.090E-06	1.868E-05	-8.034E-08
0.929	0.355	7.057E-04	5.460E-03	-3.097E-05	8.889E-06	2.718E-05	-1.037E-07
1.046	0.471	7.216E-04	7.551E-03	-6.800E-05	1.522E-05	6.504E-05	-1.804E-07
1.217	0.633	6.797E-04	9.486E-03	-1.511E-04	2.421E-05	1.485E-04	-2.996E-07
1.305	0.715	6.416E-04	1.659E-02	2.429E-03	2.842E-05	2.025E-04	-4.226E-07
1.395	0.800	6.074E-04	2.089E-02	3.784E-03	3.094E-05	2.898E-04	-5.454E-07
1.570	0.965	5.518E-04	2.990E-02	6.741E-03	3.752E-05	4.792E-04	-7.737E-07
1.831	1.200	4.624E-04	5.828E-02	1.721E-02	4.580E-05	7.224E-04	-1.114E-06
2.000	1.350	3.988E-04	7.758E-02	2.431E-02	5.067E-05	8.863E-04	-1.277E-06
2.500	1.805	3.140E-04	1.289E-01	4.024E-02	6.420E-05	1.414E-03	-1.908E-06
3.000	2.286	9.320E-05	9.752E-02	1.951E-02	9.479E-05	2.064E-03	-2.165E-06
4.000	3.087	1.135E-03	1.771E-01	1.531E-01	4.386E-03	3.699E-03	1.433E-03

M_i	M_{ej}	$M_y(^{16}O)$	$M_y(^{17}O)$	$M_y(^{18}O)$	$M_y(^{20}Ne)$	$M_y(^{22}Ne)$	$M_y(^{25}Mg)$
0.819	0.241	0	4.453E-10	-7.486E-09	0	0	0
0.877	0.300	0	2.058E-09	-2.697E-08	0	0	0
0.929	0.355	0	3.521E-09	-4.125E-08	0	0	0
1.046	0.471	0	1.451E-08	-1.243E-07	0	0	0
1.217	0.633	0	9.373E-08	-3.377E-07	0	0	0
1.305	0.715	1.903E-04	1.686E-07	-6.336E-07	0	1.389E-04	1.588E-06
1.395	0.800	2.939E-04	4.195E-07	-9.784E-07	0	2.372E-04	2.726E-06
1.570	0.965	5.114E-04	4.284E-06	-1.767E-06	0	4.981E-04	5.738E-06
1.831	1.200	1.184E-03	2.789E-05	-2.966E-06	0	1.883E-03	2.161E-05
2.000	1.350	1.602E-03	6.323E-05	-3.692E-06	0	3.096E-03	3.554E-05
2.500	1.805	2.502E-03	9.230E-05	-5.530E-06	0	6.163E-03	7.071E-05
3.000	2.286	7.931E-04	1.876E-04	-5.172E-06	0	1.773E-03	2.037E-05
4.000	3.087	3.017E-04	1.699E-04	-3.009E-05	0	2.472E-03	2.804E-05

Early-AGB, so that only the mass ejection along the TP-AGB is included in $M^{ej}_{j,AGB}$.

Tables 4 – 5 give the stellar yields $M_y(i)$ in unit of solar masses for a few chemical elements: ^{3}He, ^{4}He, ^{12}C, ^{13}C, ^{14}N, ^{15}N, ^{16}O, ^{17}O, ^{18}O, ^{22}Ne, ^{25}Mg for both values of initial metallicity. The initial mass of the star and the total mass ejected during the entire evolution are also tabulated. The negative terms correspond to those elemental species which are partially destroyed and diluted in the envelope so that their abundance in the ejected material is lower with respect to the main sequence value.

3.3. The initial-final mass relation

In Fig. 7 the final core mass M_f left after the complete ejection of the envelope is plotted against the initial mass M_i of each model for both cases $Z = 0.02$ and $Z = 0.008$. M_f is the expected value for the mass of the remnant White Dwarf (see also Table 6).

Also shown is the semi-empirical initial mass-final mass relation from Weidemann (1987) for the solar neighbourhood. Our theoretical prediction for the case $Z = 0.02$ (solid line) is in a good agreement with the observational calibration, while the prediction of Bertelli et al. (1994) (dotted line) derived by adopting the Reimers law ($\eta = 0.35$) seems to diverge quickly at increasing mass.

By comparing our theoretical results for the case $Z = 0.008$ to the corresponding ones by VW, a good agreement is also found. This indicates that, at a given age the WD mass depends on the parent metallicity.

3.4. TP-AGB lifetimes

With the adopted prescription for the mass-loss rate (§2.7), the duration of the TP-AGB phase is essentially determined by the onset of the superwind and it depends in a complex manner both on stellar mass and metallicity (see VW for a complete discussion). The predicted TP-AGB lifetimes of our models for both metallicities ($Z = 0.02$ and $Z = 0.008$) are tabulated in Table 6. In Fig. 8 we plot the theoretical TP-AGB lifetimes derived from our calculations versus the initial mass of the stars. The notable features are: i) for fixed metallicity, the duration of the TP-AGB phase is an increasing function of stellar mass in the low mass range ($M \lesssim 2.5\ M_\odot$), while for higher masses

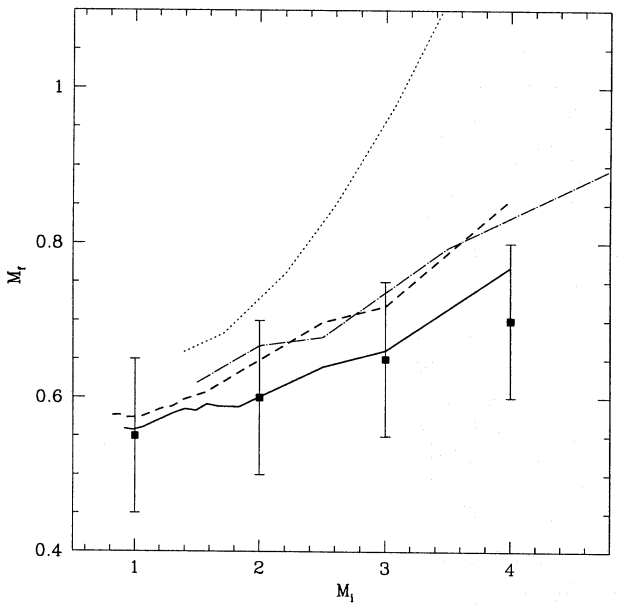

Fig. 7. Final stellar remnant mass M_f, after complete ejection of the envelope, as a function of the initial mass M_i. Filled squares (the error bars for M_f are of 0.2 $M_\odot$) correspond to the semi-empirical relation from Weidemann (1987); the solid and dashed lines represent our predicted relation, respectively, for Z = 0.02 and Z = 0.008; the dot-dashed line refers to the theoretical relation derived by VW for Z = 0.008; the dotted line correspond to the prediction of Bertelli et al. (1994) for Z = 0.02.

($M \gtrsim 2.5\ M_\odot$) the trend is reversed, and ii) at the same stellar mass the TP-AGB lifetime is significantly longer for the models with lower metallicity.

3.5. AGB pulsating stars

While on the AGB, a star may undergo large amplitude, long period pulsations. This corresponds, on the observational ground, to two classes of long period variables (LPVs), namely, the Mira stars which are optically visible and with relatively small mass-loss rates, and the OH/IR stars which are dust-enshrouded and with superwind mass-loss rates (VW).

In Fig. 9, for each mass (Z = 0.008), we plot the bolometric magnitude M_{bol} as a function of the maximum pulsation period P just prior the occurrence of each thermal pulse. From the typical trend of the tracks, we can see that during the initial part of the TP-AGB evolution $\log P$ linearly increases with M_{bol} until the onset of the superwind, at which point the period quickly grows to higher values. Such an acceleration to longer periods is more rapid for the more massive stars, according to the dependence of P on the mass and the effective temperature of the star (Eq. (9)).

The shaded areas in the figure correspond to the zones where Mira stars and OH/IR variables are detected by observations in the LMC (see Fig. 20 in VW). The overlap with our theoretical results is quite satisfactory and we may envisage that only stars more massive than $\sim 2.5 M_\odot$ are able to evolve as OH/IR variables.

Table 6. For both metallicities Z = 0.02 and Z = 0.008 and for each initial mass M_i (in $M_\odot$), the table lists the values, corresponding to the end of the TP-AGB phase, of the final mass M (in $M_\odot$), the bolometric magnitude M_{Bol}, the effective temperature T_{eff}, the TP-AGB lifetime τ_{TP-AGB} (in years).

Z	M_i	M_f	M_{Bol}	$\log T_{eff}$	τ_{TP-AGB}
0.008	0.8189	0.5771	-4.608	3.588	1650627.63
	0.8768	0.5774	-4.548	3.556	1389460.25
	0.9286	0.5740	-4.483	3.536	1191912.50
	1.0458	0.5747	-4.488	3.514	1069300.63
	1.2173	0.5859	-4.688	3.496	1086284.75
	1.3047	0.5887	-4.747	3.490	1330294.38
	1.3945	0.5972	-4.973	3.486	1440437.00
	1.5697	0.6066	-5.075	3.475	1633544.63
	1.8308	0.6323	-5.332	3.471	2455596.00
	2.0000	0.6485	-5.497	3.445	3186626.00
	2.5000	0.6978	-5.812	3.471	3078129.75
	3.0000	0.7184	-6.070	3.467	989067.75
	4.0000	0.8566	-6.450	3.476	450946.06
0.02	0.9148	0.5595	-4.128	3.511	524275.88
	0.9872	0.5580	-4.060	3.487	399459.97
	1.0655	0.5613	-4.155	3.468	528933.56
	1.1469	0.5677	-4.298	3.457	618356.19
	1.3176	0.5801	-4.560	3.436	650829.75
	1.4050	0.5849	-4.560	3.431	713341.13
	1.4919	0.5830	-4.643	3.422	718584.56
	1.5789	0.5915	-4.770	3.419	893423.50
	1.6648	0.5886	-4.830	3.410	836040.81
	1.8369	0.5877	-4.957	3.399	960659.13
	2.0000	0.6006	-5.110	3.397	1114026.00
	2.5000	0.6399	-5.468	3.400	1725436.38
	3.0000	0.6613	-5.755	3.396	579060.63
	4.0000	0.7690	-6.150	3.405	241441.58

3.6. Carbon stars

We investigate the formation of carbon stars. As already remarked, we adopt the observed luminosity function of carbon stars in the LMC as the constraint which the calibration of our model stands on. The dredge-up parameters λ and M_c^{min} (see 2.8) are estimated by demanding that the theoretical luminosity function of carbon stars calculated for Z = 0.008 suitably fits the observed one.

The adopted value of the metallicity is in agreement with the observational indications of Russell & Dopita (1990), who suggest that the present metal abundance in the LMC is $\sim$ 1/2 solar.

We take the observed histogram from GdJ, who combine the observed luminosity function of carbon stars in the LMC

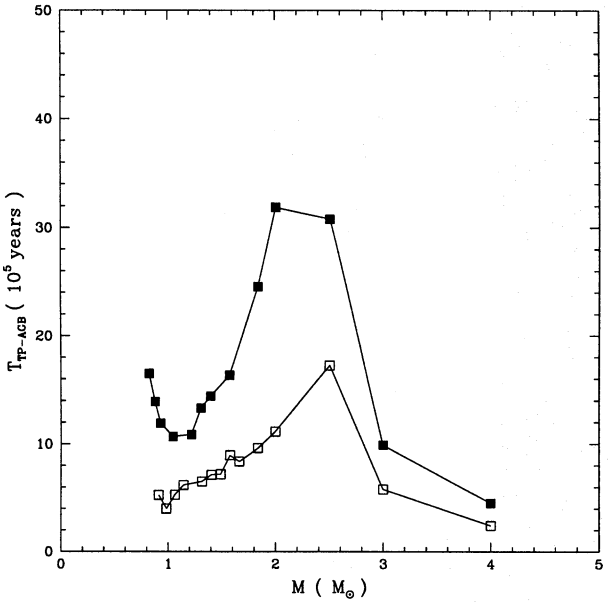

Fig. 8. Theoretical TP-AGB lifetime as a function of initial mass. Open and filled squares correspond to the case $Z = 0.02$ and $Z = 0.008$, respectively.

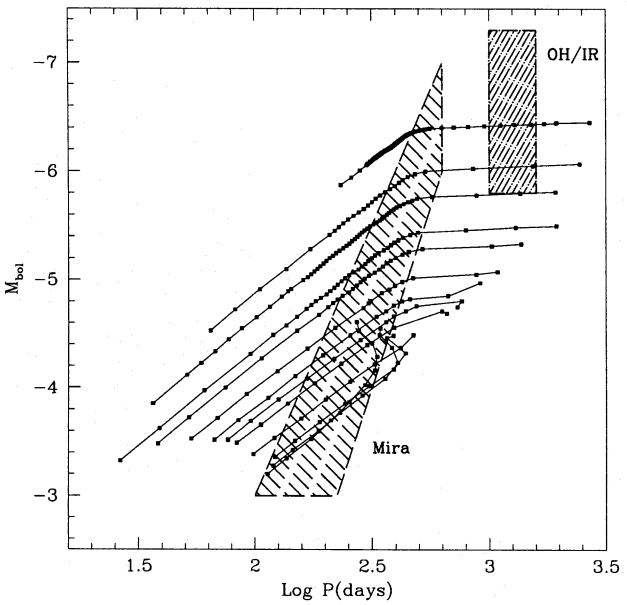

Fig. 9. M_{bol} plotted against the pulsation period P at its maximum value reached just before each He-shell flash (solid squares joined by lines) for our models with $Z = 0.008$. The shaded regions indicate the observed location of optically visible LPVs (Mira stars) and dust-enshrouded AGB stars (OH/IR stars) in the LMC.

of Cohen et al. (1981) with the data presented by Richer et al. (1979). The distance modulus of the LMC is assumed to be 18.5.

Indicating by k a specified magnitude bin with a width $\Delta M_{bol} = M_{bol}(k) - M_{bol}(k+1)$, we need to evaluate the number fraction N_k of carbon stars which are in transit at the present epoch along the k^{th} interval:

$$N_k \propto \sum_j (M_{j+1} - M_j)\Phi(M_j^*, \tau_j)\,\Delta t_{jk} \qquad (25)$$

where each term j of the summation refers to all the carbon stars with a current mass M in the range from M_j to M_{j+1}. The initial mass which corresponds to the mean value $(M_{j+1}+M_j)/2$ of the current mass is denoted by M_j^*. The quantity Δt_{jk} is the time that a star with a mass M_j spends in the k^{th} bin of luminosity; $\Phi(M_j^*, \tau_j)$ is the star formation function, that is the number of C-stars with an initial mass M_j^* and a lifetime τ_j which are born at the epoch $T_G - \tau_j$, where T_G is the age of the galaxy:

$$\Phi(M_j^*, \tau_j) = \Phi(M_j^*) = \phi(M_j^*)\psi(T_G - \tau(M_j^*)) \qquad (26)$$

It is possible to express Φ as a function of the mass only thanks to the relation between the lifetime of a star and its initial mass ($\tau_j = \tau(M_j^*)$).

In Eq. (26), $\phi(M_j^*)$ is the initial mass function giving the number of stars forming at a certain instant in the unit mass interval; $\psi(T_G - \tau(M_j^*))$ is the star formation rate representing the mass of the primordial gas that is converted into stars at the epoch $T_G - \tau(M_j^*)$.

In this study we assume the classical Salpeter (1955) law for the initial mass function, according to which the number of stars dN in the mass interval dM is given by

$$dN = AM^{-x}dM \qquad (27)$$

where $x = 2.35$ and A is a suitable normalization constant.

Moreover we adopt the age of LMC equal to 15 Gyr, and the same kind of star formation rate suggested by Bertelli et al. (1992) in their study of the CMDs of field stars in selected areas of the LMC. The star formation rate has been moderate from the beginning up to about 4.5 Gyr ago and since then a factor of ten stronger. See also Girardi et al. (1995) for a similar conclusion.

In addition to the quantities above specified, the calculation of the luminosity function of the carbon stars requires the knowledge of:

- the $M_c - L$ relation (Eqs. (1) and (2));
- the rate of evolution along the TP-AGB (Eq. (4));
- the minimum value of the initial mass for a star that is in the AGB phase at the present epoch; it corresponds to the star whose lifetime is just the age of the galaxy ($M^* \sim 0.73 M_\odot$);
- the maximum value of the initial mass of a star currently evolving along the TP-AGB phase ($5 M_\odot$);
- the minimum luminosity, as a function of the initial mass, below which the star has not yet reached the base of its TP-AGB (Fig. 10);
- the minimum luminosity, as a function of the initial mass, below which the TP-AGB star has not yet become a carbon star (Fig. 10);
- the maximum luminosity, as a function of the initial mass, reached by the star along its TP-AGB (Fig. 10).

Fig. 10 shows the bolometric magnitude M_{bol} as a function of the initial mass M_i for three characteristic stages of the AGB phase, namely the start of the TP-AGB (solid line), the transition

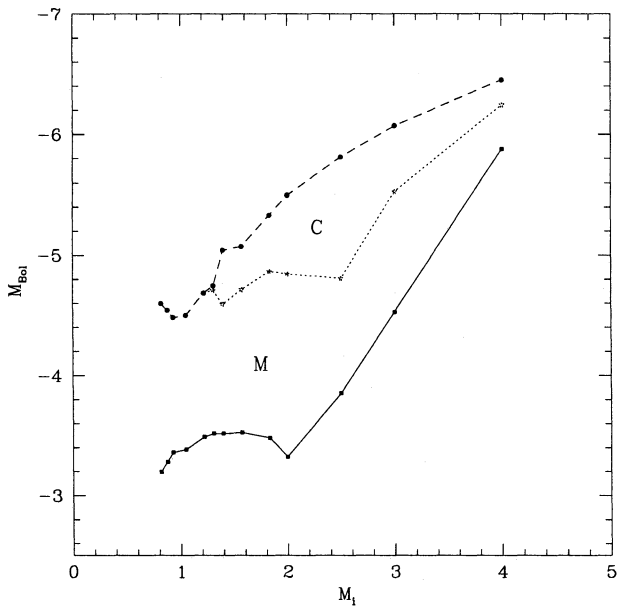

Fig. 10. Limit bolometric magnitudes vs. initial mass for the case $Z = 0.008$ (see text for further explanation of the plot).

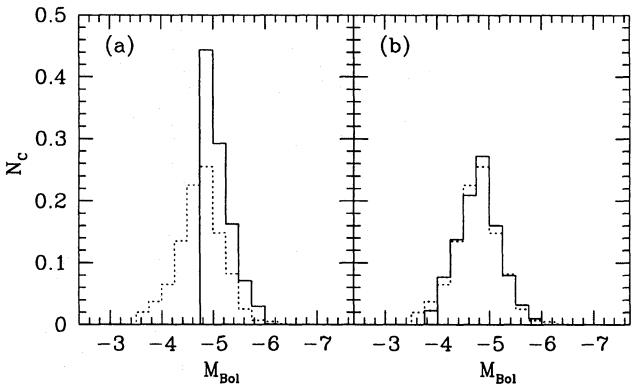

Fig. 11a and b. Luminosity function of carbon stars obtained from our models calculated at $Z = 0.008$ (solid line) without the inclusion of flash-driven luminosity variations (panel **a**), and after suitable corrections are adopted (panel **b**). The dotted lines represent the observed luminosity function of carbon stars in the LMC (GdJ).

line between the M-phase (C/O $\leq$ 1) and the C-phase (C/O $\geq$ 1) (dotted line), and the termination of the AGB phase (dashed line). The three boundary lines delimit two areas in the plane $M_{bol} - M_i$: the region marked M corresponds to the domain of the TP-AGB stars which belong to the M-class; the region marked C represents the domain of the C-class.

Note the marked dip in the dotted line around 2.5 $M_\odot$ which could mean a privileged mass range for the formation of C-stars.

At this point it is worth noticing that, with the adopted formalism for the mass loss, the minimum bolometric magnitude reached at the end of the AGB is strongly dependent on the metallicity as well as the initial mass of the star: the lower the metallicity the more luminous is the AGB tip for a given initial mass (see columns 2 and 4 in Table 6).

This feature would be quite important when attempting to estimate the age of a coeval system from the observed luminosity of AGB stars detected in it. In this sense the final AGB luminosity is not a sufficient indicator of the initial mass of the progenitor and hence the age, since the knowledge of the parent metallicity is required. To give an example, from Table 6 it turns out that both a star with initial mass $M_i \sim 0.82\ M_\odot$ and metallicity $Z = 0.008$ and a star with initial mass $M_i \sim 1.46\ M_\odot$ and metallicity $Z = 0.02$ reach approximately the same bolometric magnitude $M_{bol} = -4.61$ at the tip of the AGB. Consequently, the resulting stellar lifetimes are extremely different, corresponding to about 19.29 Gyr for the case $Z = 0.008$ and about 2.75 Gyr for the case $Z = 0.02$.

Panel (a) in Fig. 11 shows the luminosity function obtained assuming the luminosity evolution of C-stars to be fully represented by the standard $M_c - L$ relation. Evident is the disagreement between the theoretical results and the experimental histogram: the observed low-luminosity tail is totally absent in the predicted distribution.

The discrepancy is removed if we consider the effect of flash-driven luminosity variations (see Sect. 2.6) on the almost linear luminosity evolution given by the $M_c - L$ relation. In particular, the analytical inclusion of the luminosity-dip results in properly lowering the low luminosity tail of the distribution by about 1 mag. Hence the good fit as shown in panel (b) of Fig. 11.

We notice that the excess of luminous C-stars, that has been a recurrent theoretical difficulty for a long time (Iben 1981), is not predicted by our calculations, thus resulting in agreement with the observational limit in luminosity ($M_{bol} = -6$). This fact could be mainly ascribed to the combined effect of two factors: 1) the strong mass loss which makes the star to leave earlier the AGB and; 2) the lower value of the critical mass M_{up} as the consequence of adopting the convective overshoot in the evolutionary calculations (Sect. 2.1).

It is worth noticing that, on the base of our calculations, the luminosity function of carbon stars turns out to be crucially dependent only on the dredge-up parameters λ and M_c^{min}. In fact, using different initial mass functions (e.g. Salpeter 1955; Scalo 1979; Miller & Scalo 1979; Ferrini et al. 1990), while keeping fixed all other inputs, does not produce significant differences.

The sensitivity on the adopted law for the star formation rate does not seem to be dominant. Following various *reasonable* choices for ψ (e.g. a function exponentially decreasing with time; a step-function with different limit ages of the burst) the results may obviously change, but not so dramatically. To give an example, denoting by τ_B the age of the beginning of the burst, it is clear that no differences result for any adopted value $\tau_B \geq \tau_{max}$, the latter being the maximum lifetime ($\sim$ 4.1 Gyr) (corresponding to the minimum initial mass $M_{Carb}^{min} \sim 1.2\ M_\odot$) among the stars expected to become carbon stars. A certain effect may result if lowering the age of the end of the burst τ_F ($\psi \sim 0$ for ages shorter than τ_F up to now) too much below the

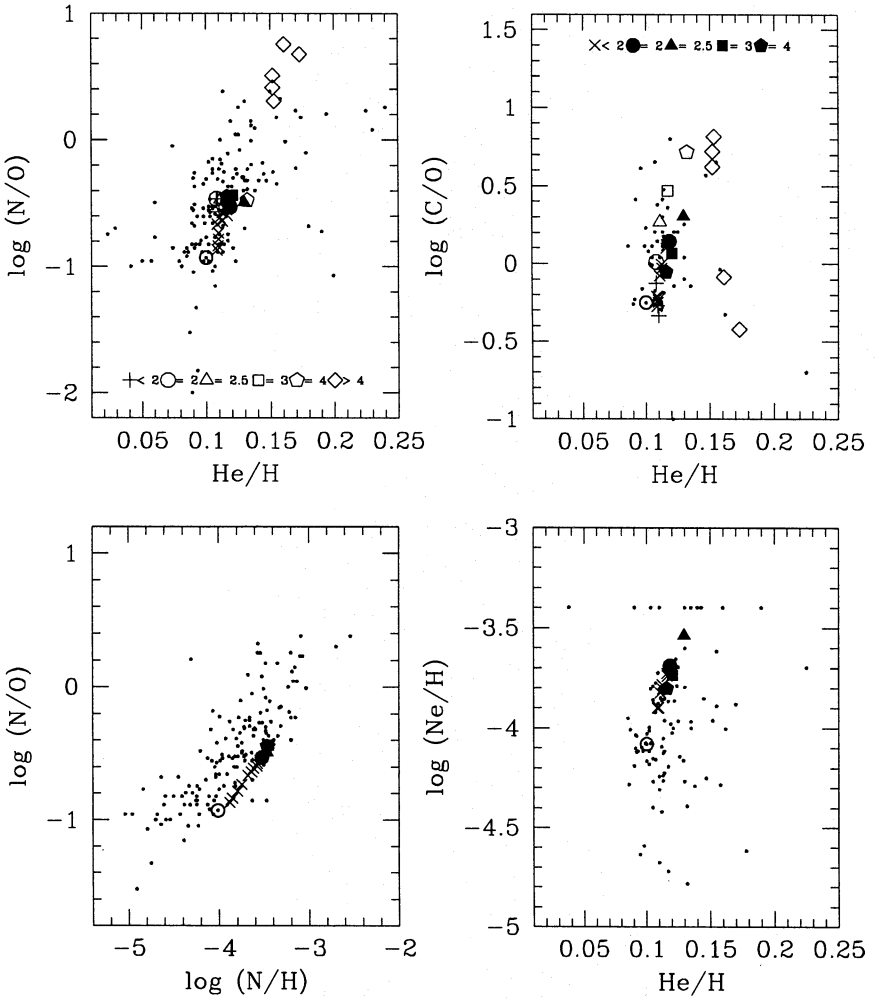

Fig. 12. Observed (points) and predicted abundance ratios of PNe in the Galaxy. Our results (legenda in the right-upper panel) and those of RV (legenda in the left-upper panel) are plotted with different symbols to evidence the initial mass (denoted by a number in units of $M_\odot$) of the progenitor star.

age of the galaxy: this would cancel the contribution of the most young (and massive) carbon stars to the high luminosity tail of the distribution.

3.7. Planetary nebulae

A further application of our TP-AGB model is the prediction of the chemical composition of planetary nebulae (PNe). For each elemental species we calculate the mean abundance (by number) in the material ejected during the last $\sim$ 5 10^4 years, that is the adopted mean lifetime of a typical PN (Zijlstra & Pottasch 1991). In Table 7 the predicted values of a few chemical ratios in PNe are given for both cases, $Z = 0.02$ and $Z = 0.008$.

A preliminary comparison between observed and predicted abundance ratios is illustrated in Fig. 12 for the galactic case (Perinotto 1991; Pasquali & Perinotto 1993) and in Fig. 13 for the LMC (Aller et al. 1987; Henry et al. 1989; Dopita & Meatheringham 1991ab; Kaler & Jacoby 1990; Meatheringham & Dopita 1991). The ratios N/O and C/O as given by RV in the case ($Z = 0.02$, $\eta = 0.333$, $\alpha = 1.5$) are also shown.

Case $Z = 0.02$

The agreement between theory and observations is rather satisfactory, except for the oxygen abundance whose experimental estimate is found to be a factor ~ 1.8 smaller than in the Sun. On the other hand, our results predict an oxygen abundance which is, at least in the more massive models, even greater than the solar value, hint of the prevailing effect of the third dredge-up with respect to the previous mixing episodes. The discrepancy is an old question that we postpone to a future investigation. The effect of the overabundance of oxygen specially reflects on the N/O – N/H diagram: the theoretical predictions of the N/O ratio are vertically shifted downward in the plot with respect to the observed data, while the evident correlation is reproduced.

Actually, the predictions fail to explain the Type I PNe, those with high N and He abundances (according to the usual classification of Peimbert 1978). The reason is that we do not find enough envelope burning in the models. The calculation of the TP-AGB evolution of the 5 $M_\odot$ model may contribute to fill the lack once the overluminosity produced by envelope burning is properly taken into account in our calculations.

A final remark concerns the abundance of Ne. Our models predict that during the TP-AGB evolution ^{22}Ne may increase

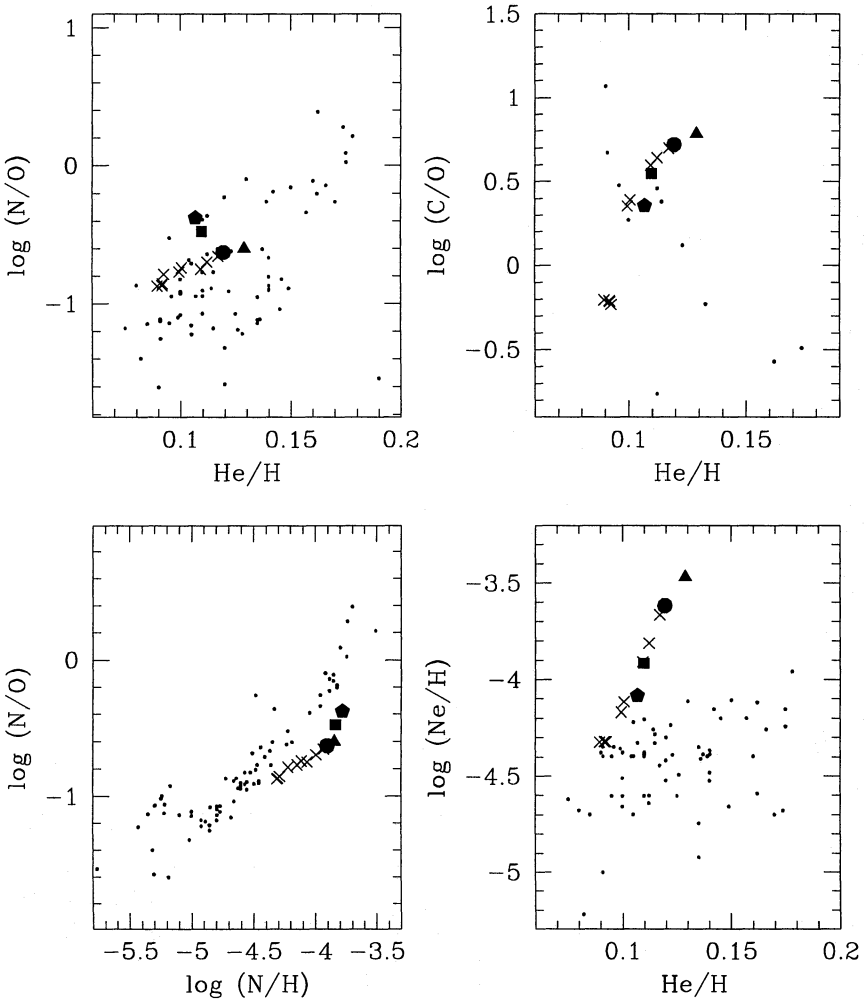

Fig. 13. Observed and predicted abundance ratios of PNe in the LMC. The adopted notation is the same as in Fig. 12.

in the envelope because of dredge-up, while ^{20}Ne is unchanged (see Sect. 2.8). This circumstance turns out attractive to interpret the slight overabundance of neon detected in bipolar PNe as pointed out by Corradi & Schwarz (1995) in their analysis of the physical properties of PNe morphological classes.

Case $Z = 0.008$

Also in this case, a general agreement is found. Note that for the C/O ratio, fewer sample data are available in the LMC than in the solar case, so that a significant comparison is harder. The predicted overestimate of the oxygen abundance with respect to the observational value is still present. The effect of envelope burning is evident in the N/O - N/H diagram for the 4 $M_\odot$ model, which clearly departs from the general smooth trend (as an increasing function of the progenitor mass) toward a greater value. In contrast to the solar case, the predicted abundances of neon for the star models of higher mass are significantly higher than the observed data, while a general agreement with the observed data is found for the lower masses.

Although the discrepancy could be ascribed to the uncertainties of the nucleosynthetic analysis, it is worth recalling the strict correlation between the PNe composition and the mass of the progenitors. In this perspective, recent investigations (Girardi et al. 1995) indicate that a strong burst of stellar formation in the LMC occurred between about 2 and 4 Gyr ago, followed by a quick decay up to now. This circumstance, together with the weighting effect from the IMF, could favour the present detection in the LMC of PNe evolved from stars of low initial mass ($1.2 \lesssim M_i/M_\odot \lesssim 1.5$).

4. Conclusions

We have developed a semi-analytical model to calculate the TP-AGB evolution of low- and intermediate-mass stars. The calibration of the two dredge-up parameters ($M_c^{\rm min} = 0.58\,M_\odot$ and $\lambda = 0.65$) is obtained by fulfilling the observational constraint of the luminosity function of C-stars in the LMC. Such values are in agreement with the recent estimates of GdJ. The dredge-up efficiency λ is much higher than found in complete evolutionary calculations of thermal pulses, thus giving evidence once more to the present deficiency in the physical treatment of the dredge-up mechanism.

The strong dependence of nuclear burning at the base of the convective envelope on the mixing length parameter α is confirmed. In this way, a properly addressed analysis of envelope

Table 7. Abundance ratios by number expected in PN-composition from calculations with $Z = 0.02$ and $Z = 0.008$. The mass of the stellar progenitor, M_i, and that of the remnant (e.g. the mass of the White Dwarf), M_{WD}, are indicated in solar units.

Z	M_i	M_{WD}	He/H	log(C/O)	log(N/O)	log(N/H)	log(O/H)	log(Ne/H)
0.02	0.915	0.559	0.1086	-0.2084	-0.8688	-3.8798	-3.0110	-3.8980
	0.987	0.558	0.1092	-0.2183	-0.8380	-3.8486	-3.0106	-3.8977
	1.066	0.561	0.1096	-0.2336	-0.7837	-3.7939	-3.0103	-3.8973
	1.147	0.568	0.1095	-0.2489	-0.7346	-3.7451	-3.0104	-3.8975
	1.318	0.580	0.1084	-0.2756	-0.6657	-3.6777	-3.0120	-3.8991
	1.405	0.586	0.1124	-0.0290	-0.6388	-3.6381	-2.9994	-3.8044
	1.492	0.585	0.1108	-0.0757	-0.6121	-3.6149	-3.0028	-3.8234
	1.665	0.591	0.1123	-0.0027	-0.5737	-3.5729	-2.9992	-3.7841
	1.837	0.586	0.1158	0.1008	-0.5514	-3.5452	-2.9938	-3.7267
	2.000	0.604	0.1185	0.1441	-0.5293	-3.5228	-2.9935	-3.6889
	2.500	0.637	0.1295	0.3058	-0.4899	-3.4688	-2.9789	-3.5395
	3.000	0.661	0.1206	0.0667	-0.4356	-3.4481	-3.0125	-3.7359
	4.000	0.769	0.1160	-0.0530	-0.4453	-3.4672	-3.0219	-3.8027
0.008	0.819	0.578	0.0895	-0.2047	-0.8720	-4.3091	-3.4371	-4.3244
	0.877	0.577	0.0917	-0.2091	-0.8694	-4.3041	-3.4347	-4.3219
	0.929	0.574	0.0919	-0.2136	-0.8543	-4.2889	-3.4347	-4.3219
	1.046	0.575	0.0925	-0.2319	-0.7859	-4.2199	-3.4341	-4.3213
	1.217	0.584	0.0995	0.3545	-0.7688	-4.1481	-3.3793	-4.1696
	1.305	0.589	0.1006	0.3910	-0.7403	-4.1121	-3.3718	-4.1168
	1.395	0.595	0.1093	0.5968	-0.7498	-4.0648	-3.3149	-3.9084
	1.570	0.604	0.1121	0.6412	-0.6967	-3.9938	-3.2971	-3.8124
	1.831	0.630	0.1171	0.6981	-0.6547	-3.9325	-3.2779	-3.6651
	2.000	0.650	0.1194	0.7194	-0.6288	-3.9022	-3.2733	-3.6179
	2.500	0.695	0.1289	0.7841	-0.6003	-3.8435	-3.2433	-3.4685
	3.000	0.714	0.1097	0.5494	-0.4756	-3.8349	-3.3594	-3.9160
	4.000	0.913	0.1068	0.3562	-0.3766	-3.7784	-3.4019	-4.0844

burning could be potential mean to derive indications on the probable inadequacy of the convective theory, by constraining it to satisfy the experimental requests on the surface chemical compositions of AGB stars.

Moreover, we recall that, envelope burning, when efficiently operating, can produce a significant deviation of the star from the standard $M_c - L$ relation and this effect should be taken into account in a coherent theoretical analysis. Actually, we do not include the contribution of nuclear burning to the stellar luminosity and that could be a future improvement of our model.

A notable feature coming from our results is the significant dependence of the initial-final mass relation on the metallicity. It could be employed in evolutionary models of elliptical galaxies as a tool to investigate the question on the origin of the ultra-violet excess detected in these systems and its correlation with metallicity, phenomenon generally attributed to the post-AGB phases (Bressan et al. 1994). In this perspective, the extension of our TP-AGB calculations to other classes of metallicity could be an interesting future development of our study.

Acknowledgements. We are grateful to our referee, prof. P.R. Wood, for many constructive critical comments on this work. We also thank: M. Perinotto and L.M. Romano Corradi for interesting conversations on planetary nebulae; R. Gallino for his kind interest and useful remarks. Special thanks to Léo Girardi for his stimulating support. This study has been financed by the Italian Ministry of University, Scientific Research and Technology (MURST) and the Italian Space Agency (ASI).

References

Aller L.H., Keyes C.D., Maran S.P., Gull T.R., Michalitsianos A.G., Stecher T.P., 1987, ApJ 320, 159
Bertelli G., Mateo M., Chiosi C., Bressan A., 1992, ApJ 388, 400
Bertelli G., Bressan A., Chiosi C., Fagotto F., Nasi E., 1994, A&AS 106, 275
Bowen G.H., 1988, ApJ 329, 299
Blöcker T., 1995, A&A 297, 727
Blöcker T., Schönberner D., 1991, A&A 244, L43
Boothroyd A.I., Sackmann I.-J., 1988a, ApJ 328, 632 (BSa)
Boothroyd A.I., Sackmann I.-J., 1988b, ApJ 328, 641 (BSb)
Boothroyd A.I., Sackmann I.-J., 1988c, ApJ 328, 653 (BSc)
Boothroyd A.I., Sackmann I.-J., 1988d, ApJ 328, 671 (BSd)
Boothroyd A.I., Sackmann I.-J., 1992, ApJ 393, L21
Boothroyd A.I., Sackmann I.-J., Ahern S.C, 1993, ApJ 416, 762
Bressan A., Fagotto F., Bertelli G., Chiosi C., 1993, A&AS 100, 674
Bressan A., Fagotto F., Chiosi C., 1994, ApJS 94, 63
Busso M., Gallino R., Lambert D.L., Raiteri C.M., Smith V.V., 1992, ApJ 399, 218

Castor J.I., Abbot D.C., Klein R.I., 1975, ApJ 195, 157
Caughlan, G.R., Fowler, W.A., 1988, Atomic Data Nuc. Data Tables 40, 283
Chiosi C., Bertelli G., Bressan A., 1992, ARA&A 30, 235
Clayton D.D., 1983, Principles of Stellar Evolution and Nucleosynthesis, University of Chicago Press, Chicago and London
Cohen J.G., Frogel J.A., Persson S.E., Elias J.H., 1981, ApJ 249, 481
Corradi R.L.M., Schwarz H.E., 1995, A&A 293, 871
Cox J.P., Giuli R.T., 1968, in: Principles of Stellar Structure, Gordon and Breach Science Publishers Inc., New York, p. 281
Dopita M.A., Meatheringham S.J., 1991a, ApJ 367, 115
Dopita M.A., Meatheringham S.J., 1991b, ApJ 377, 480
Fagotto F., Bressan A., Bertelli G., Chiosi C., 1994, A&AS 104, 365
Ferrini F., Penco U., Palla F., 1990, A&A 231, 391
Gallino R., Busso M., Picchio G., Raiteri C.M., Renzini A., 1988, ApJ 334, L45-L49
Girardi L., Chiosi C., Bertelli G., Bressan A., 1995, A&A 298, 87
Graboske H.C., Witt H.E., Grossman A.S., Cooper, M.S., 1973, ApJ 181, 457
Groenewegen M.A.T., de Jong T., 1993, A&A 267, 410 (GdJ)
Groenewegen M.A.T., de Jong T., 1994a, A&A 282, 127
Groenewegen M.A.T., de Jong T., 1994b, A&A 283, 468
Hollowell D.E., 1987, in: Kwok S. and Pottasch S.R. (eds) Late Stages of Stellar Evolution, Reidel, Dordrecht, p. 239
Hollowell D.E., Iben I. Jr., 1988, in IAU Colloquium 108, Atmospheric Diagnostic of Stellar Evolution, Springer-Verlag, Berlin
Havazelet D., Bakart Z., 1979, ApJ 233, 589
Henry R.B.C., Liebert J., Boroson T.A., 1989, ApJ 339, 872
Iben I. 1977, ApJ 217, 788
Iben I., 1981, ApJ 246, 278
Iben I Jr. 1991, ApJS 76, 55
Iben I., Renzini A., 1983, Ann. Rev. Astr. Ap. 21, 271
Iben I., Renzini A., 1984, Phys. Rep. 105, 329
Iben I, Truran J.W., 1978, ApJ 220, 980 (IT)
Kaler J.B., Jacoby G.H., 1990, ApJ 362, 491
Lattanzio J.C., 1986, ApJ 311, 708
Lattanzio J.C., 1989a, ApJ 344, L25
Lattanzio J.C., 1989b, in: Johnson H.RT., Zuckerman B. (eds.) Late Stages of Peculiar Red Giant Stars, Cambridge Univ. Press, Cambridge, p. 161
Lattanzio J.C., 1989c, ApJ 347, 989
Lattanzio J.C., 1992, Proc. Astron. Soc. Austr. 10, 120
Meatheringham S.J., Dopita M.A., 1991, ApJS 75, 407
Miller G.E., Scalo J.M., 1979, ApJS 41, 513
Paczynski B., 1970, Acta Astr. 20, 47
Paczynski B., 1975, ApJ 202, 558
Pasquali A., Perinotto M., 1993, A&A 280, 581
Peimbert M., 1978, in: Tersian Y. (ed) Proc. IAU Symp. 76, Planetary Nebulae, Reidel, Dordrecht, p. 215
Perinotto M., 1991, ApJSS 76, 687
Reimers D., 1975, Mem. Soc. R. Sci. Liege 6 (8), 369
Renzini A., 1977, in: P. Bouvier, A. Maeder (eds) Advanced Stages of Stellar Evolution, Geneva Observatory, Geneva, p. 151
Renzini A., Fusi Pecci F., 1988, ARA&A 26, 199
Renzini A., Voli M., 1981, A&A 94, 175 (RV)
Russell S.C., Dopita M.A., 1990, ApJS 74, 93
Richer H.B., Olander N., Westerlund B.E., 1979, ApJ 230, 724
Sackmann I.-J., Boothroyd A.I., 1992, ApJ 392, L71-L74
Salpeter E.E., 1955, ApJ 121, 161
Scalo J.M., 1986, Fundam. Cosmic Phys. 11, 1
Straniero O., Gallino R., Busso M., et al., 1995, A&A 440, L85-L87
Vassiliadis E., Wood P.R., 1993, ApJ 413, 641 (VW)
Weidemann V., 1987, A&A 188, 74
Wood P.R., Zarro D.M., 1981, ApJ 247, 247
Zijlstra A.A., Pottasch S.R., 1991, A&A 243, 478

This article was processed by the author using Springer-Verlag LaTeX A&A style file version 3.